Marine Biodiversity (2019) 49:2167–2192
https://doi.org/10.1007/s12526-018-0906-5

SENCKENBERG

MEIOLANZA

Diversity and evolution of the stygobitic *Speleonerilla* nom. nov. (Nerillidae, Annelida) with description of three new species from anchialine caves in the Caribbean and Lanzarote

Katrine Worsaae[1] · Brett C. Gonzalez[1] · Alexandra Kerbl[1] · Sofie Holdflod Nielsen[1] · Julie Terp Jørgensen[1] · Maickel Armenteros[2] · Thomas M. Iliffe[3] · Alejandro Martínez[1,4]

Received: 30 December 2017 / Revised: 5 June 2018 / Accepted: 7 June 2018 / Published online: 27 July 2018

Abstract

Anchialine caves have revealed a variety of highly adapted animals including several records of nerillid annelids. However, only one stygobitic lineage, *Speleonerilla* nom. nov. (previously known as *Longipalpa*), seems obligate to this environment. We here provide new information on this lineage including the description of three new species, two new records, and the first phylogeny of the genus. All species have been collected from the water column of anchialine caves in the Caribbean, Bermuda, and Canary Islands, contrary to their benthic and interstitial nerillid relatives. New species were described combining light, scanning electron, and confocal laser scanning microscopy and named after traditional dances from their corresponding countries. *Speleonerilla isa* sp. n. is morphologically the most divergent species, characterized by the presence of nine segments, two pairs of spermioducts, and parapodial cirri present on all segments. *Speleonerilla calypso* sp. n. and *S. salsa* sp. n. are mainly distinguished from *S. saltatrix* by the presence of one additional pair of nephridia and are diagnosed based on unique combinations of characters including the specific arrangements of trunk ciliation, parapodial cirri, and number of chaetae. Two additional records from anchialine caves in Northeast Cuba and México were not described due to limited available material. Phylogenetic analyses of four molecular markers recovered the East Atlantic *S. isa* as sister to a clade containing the West Atlantic species, the interrelationship of which did not further reflect the geographical distances within the Caribbean. Evolutionary adaptations are discussed, such as the long ciliated palps and pygidial lobes of *Speleonerilla* used for swimming and their high tolerance to changing salinities when apparently feeding on bacteria in the halocline of the anchialine cave systems.

Keywords Interstitial · Cave fauna · Meiofauna · Troglomorphism · Stygofauna

Introduction

The meiofaunal family Nerillidae Levinsen, 1883 consists of 51 described species classified into 15 genera bearing seven to nine segments (Worsaae 2014). Nearly all species are known from marine or brackish environments from throughout the world (except for Antarctica), occurring from the intertidal zone to abyssal depths (Worsaae and Kristensen 2005; Worsaae and Rouse 2009). The only described freshwater species is *Troglochaetus beranecki* Delachaux, 1921, which has been found in both hyporheic and subterranean localities throughout the Northern Hemisphere (Jouin 1973; Morselli et al. 1998; Pennak 1971; Plesa 1977; Sambugar 2004; Särkkä and Mäkela 1998). Although members of the Nerillidae are found in varying environments, the highest diversity is found within interstitial habitats (Worsaae 2005a). Remarkably,

Communicated by P. Martínez Arbizu

✉ Katrine Worsaae
kworsaae@bio.ku.dk

[1] Marine Biological Section, Department of Biology, University of Copenhagen, Universitetsparken 4, 2100 Copenhagen, Denmark

[2] Centro de Investigaciones Marinas, Universidad de La Habana, 16 # 114, Playa, CP11300 Havana, Cuba

[3] Department of Marine Biology, Texas A&M University at Galveston, 1001 Texas Clipper Road, Galveston, TX 77553, USA

[4] Institute of Ecosystem Study, Italian National Research Council, Largo Tonolli, 50, Verbania, Italy

several nerillids are found in numerous types of marine subterranean environments, including both marine and anchialine caves (Curini-Galletti et al. 2012; Martínez et al. 2009; Núñez et al. 1997; Sterrer and Iliffe 1982; Tilzer 1970; Worsaae et al. 2009).

Whereas marine caves hold high levels of exchange with the surrounding oceanic waters, anchialine caves are characterized by the presence of density-stratified water bodies of varying salinities, often steeply separated by haloclines, which are only challenged by subterranean tidal currents (Iliffe and Kornicker 2009; Gerovasileiou et al. 2016). Photosynthetic primary production in anchialine caves is limited to inland entrance pools, and the organic matter present in these cave systems may enter the system with marine tidal oscillations and percolation from overlying soil layers or be locally produced by chemoautotrophic bacteria (Gonzalez et al. 2011; Brankovits et al. 2017). Despite these specific ecological conditions, anchialine caves are inhabited by a comparatively rich and diverse fauna, characterized by high levels of endemism (Iliffe and Bishop 2009; Martínez et al. 2016).

Anchialine cave-exclusive species are termed stygobites and usually present a set of common adaptations collectively called "troglomorphisms," which typically include the absence or reduction of eyes and pigmentation, elongation of body appendages, ability to endure starvation, and decreased metabolic rates (Iliffe and Bishop 2009). Crustaceans typically dominate the anchialine fauna, but recent studies have revealed an increased number of specialized lineages of annelids exclusive to caves, although only some of these can be characterized as stygobites (Gerovasileiou et al. 2016). For instance, several nerillids have been recorded in anchialine caves throughout the Caribbean, Bermuda, and the Canary Islands, but most of these records correspond to genera often found in the ocean and comprise benthic species morphologically similar to their marine relatives (Sterrer and Iliffe 1982; Núñez et al. 1997; Worsaae et al. 2009). In contrast, the only described species of *Longipalpa*, herein designated by the new name *Speleonerilla saltatrix* (Worsaae et al. 2004), presents a highly divergent morphology and a unique lifestyle compared to the remaining species of the family (Worsaae et al. 2004; Worsaae 2005a, b). Instead of gliding among the sand grains while feeding on detritus as most interstitial nerillids, *S. saltatrix* propels through the water column of anchialine caves by ciliary motion of their densely ciliated paired pygidial lobes, while using a pair of extremely long lateroventral palps to feed on suspended organic matter (Worsaae et al. 2004). Due to these unique adaptations for a swimming lifestyle, it is unlikely that *S. saltatrix* can survive outside of caves given the stronger currents and predators of the open marine waters; the species hereof representing a highly specialized, stygobitic nerillid.

While *S. saltatrix* has been so far the only described member of the genus, cave diving exploration in several unconnected localities throughout the Caribbean and the Canary Islands has yielded disparate new records of *Speleonerilla*. In this study, we describe three new species of *Speleonerilla* combining light, scanning electron, and confocal laser scanning microscopy, while reporting two additional populations for which only limited material was available and full descriptions could not be conducted. We also present the first phylogeny of the genus based on four molecular markers collected from all available material. These results are combined to discuss putative morphological adaptations of *Speleonerilla* to anchialine cave environments, as well as proposing alternative pathways for the diversification of this enigmatic group of microscopic, stygobitic annelids on both sides of the Atlantic.

Materials and methods

Collecting and processing of samples

Samples were collected from five different cave localities: the limestone caves Cherokee Road Extension Blue Hole "Magical Sinkhole" (Abaco, Bahamas), Casimba El Brinco (Ciénaga de Zapata, Matanzas, Cuba), Hoyo Verde (Gibara, Holguín, Cuba), and Cenote 27 Steps "Sistema Ah Kax Ha (Otra Avicola)" (Akumal, Quintana Roo, México). These caves are all characterized by high stratification in their water column, including freshwater, brackish, and saltwater layers separated by steep haloclines associated with redox layers and chemoautotrophic bacterial production (e.g., Gonzalez et al. 2011). In contrast, La Corona lava tube (Lanzarote, Canary Islands, Spain) is poorly stratified, lacks significant amounts of freshwater, and is affected by noticeable tidal currents bringing organic matter into the system (Wilkens et al. 2009).

All samples were collected using conical plankton nets with a diameter of 20–30 cm and a mesh size of 60 or 300 μm. Nets were towed by cave divers both within and below the halocline of each cave. Animals were sorted and photographed alive in the field using a Nikon D300 mounted on an Olympus SZX16 stereomicroscope. Prior to fixation, all animals were anesthetized with a 1:1 isotonic solution of $MgCl_2$ and seawater.

Morphological examinations

Morphology was assessed using scanning electron microscopy (SEM), confocal laser scanning microscopy (CLSM), and light microscopy (LM).

Specimens examined using SEM were fixed in a solution of 2% glutaraldehyde in 0.1 M sodium cacodylate buffer (for

24 h at 4°C, and transferred to 0.1 M sodium cacodylate buffer), post-fixed in 2% osmium tetroxide (1 h), rinsed in Milli-Q water, dehydrated through an ascending ethanol series from 20 to 100%, and transferred to 100% acetone. Specimens in acetone were then critical point-dried, mounted on aluminum stubs, sputter-coated with platinum palladium (high resolution sputter coater JFC-2300HR), and examined with a JEOL JSM-6335F field emission scanning electron microscope at the Natural History Museum of Denmark, University of Copenhagen.

Specimens examined with CLSM were fixed using 2% paraformaldehyde in phosphate buffer solution with 0.2 M of sucrose (PFA, for 24 h at 4°C). Fixed specimens were subsequently rinsed over 4 h in phosphate buffer (PBS with 0.2 M sucrose) and stored at 4°C after the addition of 0.05% NaN_3. Before immunostaining, specimens were preincubated for 1 h in PTA (PBS containing 0.1% Triton X-100 and 0.25% bovine serum albumin). Samples were then incubated in the primary antibody (monoclonal mouse anti-acetylated α-tubulin; T6793, Sigma; dilution 1:200 in PTA) for ca. 16 h at room temperature, washed six times over 2 h in PBS, and incubated in secondary antibodies (anti-mouse cyanamine (CY5), 115-175-062, Jackson ImmunoResearch; dilution 1:400) for ca. 16 h in the dark at room temperature. Specimens were then washed six times over 2 h and incubated with DAPI (2201.08, Sigma; dilution 1:100) or CYBR-green (S4438, Sigma; dilution 1:100). Stained specimens were mounted between two coverslips with Fluoromount-G (Southern Biotech) or Vectashield (Vector Laboratories). Specimens mounted in Fluoromount-G were stored 24 h at 4 °C and then at least 24 h at −20°C prior to CLSM. Specimens mounted in Vectashield were analyzed with CLSM immediately after mounting. Preparations were investigated with an Olympus Fluoview FV-1000 CLSM (Worsaae Lab, University of Copenhagen, Denmark), with Fluoview v4.0 software. Maximum intensity projection of z-stacks and various rendering analyses were conducted with Imaris 7.7 (Bitplane Scientific Software).

Light microscopy observations were done both on glutaraldehyde- and paraformaldehyde-fixed specimens mounted in glycerol. Measurements and photographs were taken using an OLYMPUS DP73 camera mounted on an Olympus IX70 inverted compound microscope equipped with CellSens Entry v.1.9 software. Measurements were taken from scaled SEM or CLSM pictures using ImageJ 1.47v (Schneider et al. 2012) and Olympus CellSens Entry v.1.9 software.

All types (holo- and paratypes, both on stubs and mounted in glycerol) are deposited at the Natural History Museum Denmark (NHMD-218142–NHMD-21855, NHMD-218167–NHMD-218182).

Molecular analyses

Six species of *Speleonerilla* and four nerillid outgroups were included in the phylogenetic analyses (see Table 1). DNA was extracted using a Qiagen DNeasy Tissue and Blood kit following the protocols provided by the manufacturer. DNA elution (~ 100–160 μL) was repeated twice to maximize the amount of DNA yielded. Ribosomal markers 18S rRNA (ca. 1800 bp) and 28S rRNA (ca. 1100 bp), as well as the protein coding markers cytochrome c-oxidase subunit I (COI, ca. 650 bp), and histone 3 (H3, ca. 330 bp) were amplified. Primers for 18S rRNA included 18S-1F/18S-5R (Giribet et al. 1996), G51/G747 (Hillis and Dixon 1991; Ibrahim et al.

Table 1 Data obtained for *Speleonerilla* spp. and four outgroups of the phylogenetic analyses

Species	Locality	18S	28S	COI	H3	LM	SEM	CLSM
Speleonerilla saltatrix	Roadside Cave, Bermuda	MH395334	MH395344	MH395363	MH395354	x	x	x
Speleonerilla calypso	Cherokee Road Extension Blue Hole, Abaco, Bahamas	MH395335	MH395345	MH395365	MH395355	x	x	x
Speleonerilla isa	Túnel de la Atlántida, Lanzarote, Spain	MH395341	MH395346	MH395366	MH395357	x	x	x
Speleonerilla salsa	El Brinco cave, Ciénaga de Zapata, South Cuba	MH395343	MH395349	MH395362	–	x	x	x
Speleonerilla sp. A	Hoyo Verde cave, Holguin, Northeast Cuba	MH395339	MH395348	MH395367	MH395356	x	x	–
Speleonerilla sp. B	Taj Mahal & 27 Steps Cenotes, Akumal, México	MH395338	MH395347	MH395364	–	x	–	x
Mesonerilla armoricana	Grotta di Nereo, West Sardinia, Italy	MH395337	MH395351	MH395368	MH395359	x	–	–
Mesonerilla fagei	Primel, Roscoff, France	MH395336	MH395350	–	MH395360	x	–	–
Leptonerilla prospera	Walsingham Cave, Bermuda	MH395342	MH395352	MH395369	MH395358	x	–	–
Leptonerilla sp.	Scripps Aquarium, San Diego, USA	MH395340	MH395353	MH395370	MH395361	x	–	–

2011), and G952/G944 (Cohen et al. 2004; Lovejoy and Potvin 2011); for 28S rRNA, it included primers G758/G1275 (Brown et al. 1999; Markmann 2000); primers for COI included LCO1490/HCO2198 (Folmer et al. 1994) and dgLCO1490/dgHCO2198 (Meyer 2003); and primers for histone 3 included H3aF/H3aR (Colgan et al. 1998). Polymerase chain reactions (PCR) followed a profile optimized during previous studies (see above) and used a Bio-Rad S100 Thermal Cycler. Amplified products were resolved in agarose gels, purified using EZNA Cycle-Pure kit (Omega Bio-tek), and sequenced by Macrogen Europe. Quality assessments of chromatograms and contig assemblages were done using Sequencher v. 4.10.1 (GeneCodes Corporation), and all contigs were subsequently blasted to check for contamination.

Sequences for each gene were visualized using BioEdit (Hall 1999) and aligned using the MAFFT online platform (Katoh et al. 2010). Protein coding genes COI and H3 were translated into amino acids and checked for indels and stop codons in Mesquite v.3.5. The interactive refinement algorithm Q-INS-I (Katoh and Toh 2008) was selected for alignments of 18S rRNA and 28S rRNA, as it incorporates information on the secondary structure of each ribosomal gene. The option "nwildcard" was selected for both cases, as it does not designate missing data as gaps. Gene fragments COI and H3 were constant in length and therefore trivial in alignment, but we checked for directionality using the quick interactive refinement algorithm L-INS-I (Katoh et al. 2005). Individual gene datasets were concatenated using Sequence Matrix (Vaidya et al. 2011).

Concatenated molecular datasets were analyzed using maximum likelihood and Bayesian methods. Maximum likelihood (ML) partitioned analyses were conducted using RAxML version 7.2.8 (Stamatakis 2006). A default general time reversible model with corrections for a discrete gamma distribution (GTR + Γ) was specified for each partition. Nodal support was estimated via nonparametric bootstrapping (Felsenstein 1985) with 1000 replicates and a GTR + Γ model. Bayesian analyses (BA) were performed using MrBayes version 3.2.5 (Ronquist and Huelsenbeck 2003). Datasets were run with four independent analyses using four chains (three heated and one cold) for 60 million generations, with sampling every 1000 generations. Burnin was set to 20 million. Convergence of all Monte Carlo Markov chain runs was assessed using TRACER v1.6.0 (Rambaut and Drummond 2007). Prior to Bayesian analyses, jModelTest (Posada 2008) was used to infer the optimal evolutionary model for each gene, which was selected using the corrected Akaike information criterion (AICc) (Posada and Buckley 2004). A GTR + Γ and a proportion of invariable sites (GTR + I + Γ) were selected for 18S rRNA, 28S rRNA, and COI, while a GTR model with gamma distribution (GTR + Γ) was implemented for H3. All analyses were run on the CIPRES science gateway (Miller et al. 2010).

Fig. 1 *Speleonerilla calypso* sp. n. Light microscopy images of **a** the entire specimen with both palps in dorsal view; **b** detail of parapodial cirrus on segment V; **c** detail of chaetae with shaft, extension shaft and blade; **d** detail of glandular cells on dorsal surface of segments III–IV; **e** maximum intensity projection of CLSM image stack showing segmentally arranged nephridia, oviducts, and spermioducts in ventrolateral view (pink—acetylated α-tubulin-like immunoreactivity, cyan—DAPI). bl, chaetal blade; cec, cirumesophageal connective; cs, chaetal shaft; eg, egg; es, extension shaft; gc, glandular cells; ne1–3, nephridium 1–3; od, oviduct; pa, palps; pc, parapodial cirrus; pl, pygidial lobe; sd, spermioduct; vlnv, ventrolateral nerve cord; I–VIII, segments I–VIII

Results

Family **Nerillidae** Levinsen, 1883

Genus ***Speleonerilla*** Worsaae, Sterrer & Iliffe, 2018. *Speleonerilla* is new replacement name for *Longipalpa* Worsaae, Sterrer & Iliffe, 2004 [preoccupied: *Longipalpa* Pagenstecher, 1900 (Insecta: Lepidoptera) (see Pagenstecher,1900)]. ZooBank number: urn:lsid:zoobank.org: act:92DDA88E-8A3C-4A3F-B13E-211DC0576F17.

Emended diagnosis (from Worsaae et al. 2004) Nerillids with eight or nine chaetigerous segments. Prostomium with two very long cirriform ventrolateral palps (equal to body length), no eyes, three short antennae. Pygidium with two filiform cirri, a dorso-terminal anus between two unique, densely ciliated lobes. All segments with long compound chaetae. Each body segment with transverse ventral and dorsal rows containing up to eight ciliary tufts. Two or three pairs of segmental nephridia opening in segments III and IV, or III, IV, and V. Hermaphroditic with one or two pairs of spermioducts opening in segments VII, or VI and VII, and one pair of oviducts opening in segment VIII.

Remarks A new generic name, *Speleonerilla* nov. nom., is here proposed in order to eliminate the homonymy between the genera *Longipalpa* Pagenstecher, 1900, junior synonymy of *Bytharia* Walker, 1865 (Geometridae, Lepidoptera) (see Walker, 1865) and *Longipalpa* Worsaae, Sterrer and Iliffe, 2004 (Nerillidae, Annelida).

Speleonerilla calypso sp. n.
Figures 1, 2, and 3; Tables 1, 2, 3, and 4

Type material Holotype (NHMD-218142) on SEM stub, 501 μm long, Cherokee Road Extension Blue Hole "Magical Sinkhole," Bahamas, Abaco Island, water column,

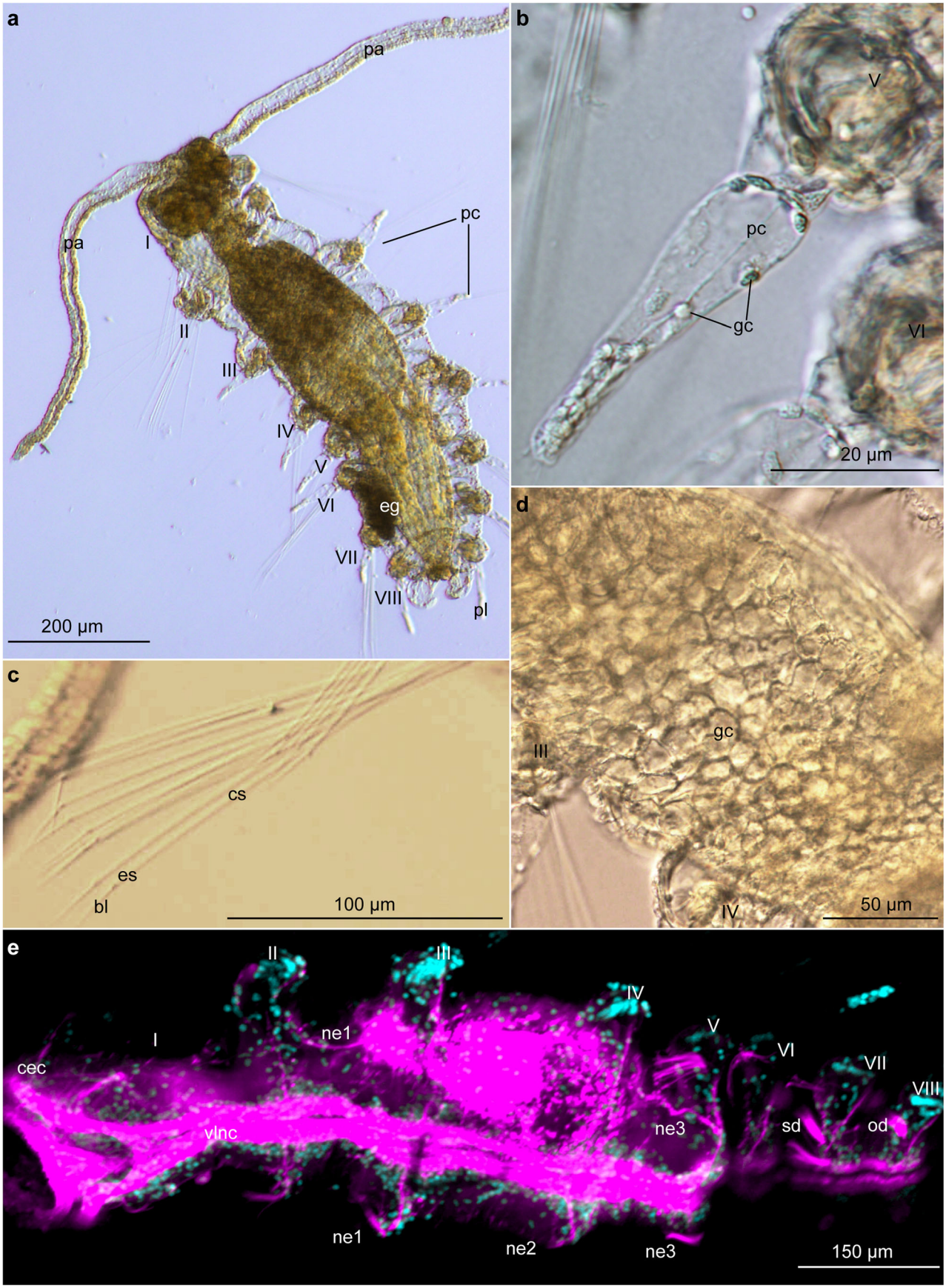
a
pa
pc
pa
I
II
III
IV
V
VI
eg
VII
VIII
pl
200 µm
b
V
pc
gc
VI
20 µm
c
cs
es
bl
100 µm
d
gc
III
IV
50 µm
e
II
III
IV
V
VI
VII
VIII
I
ne1
cec
vlnc
ne3
sd
od
ne1
ne2
ne3
150 µm

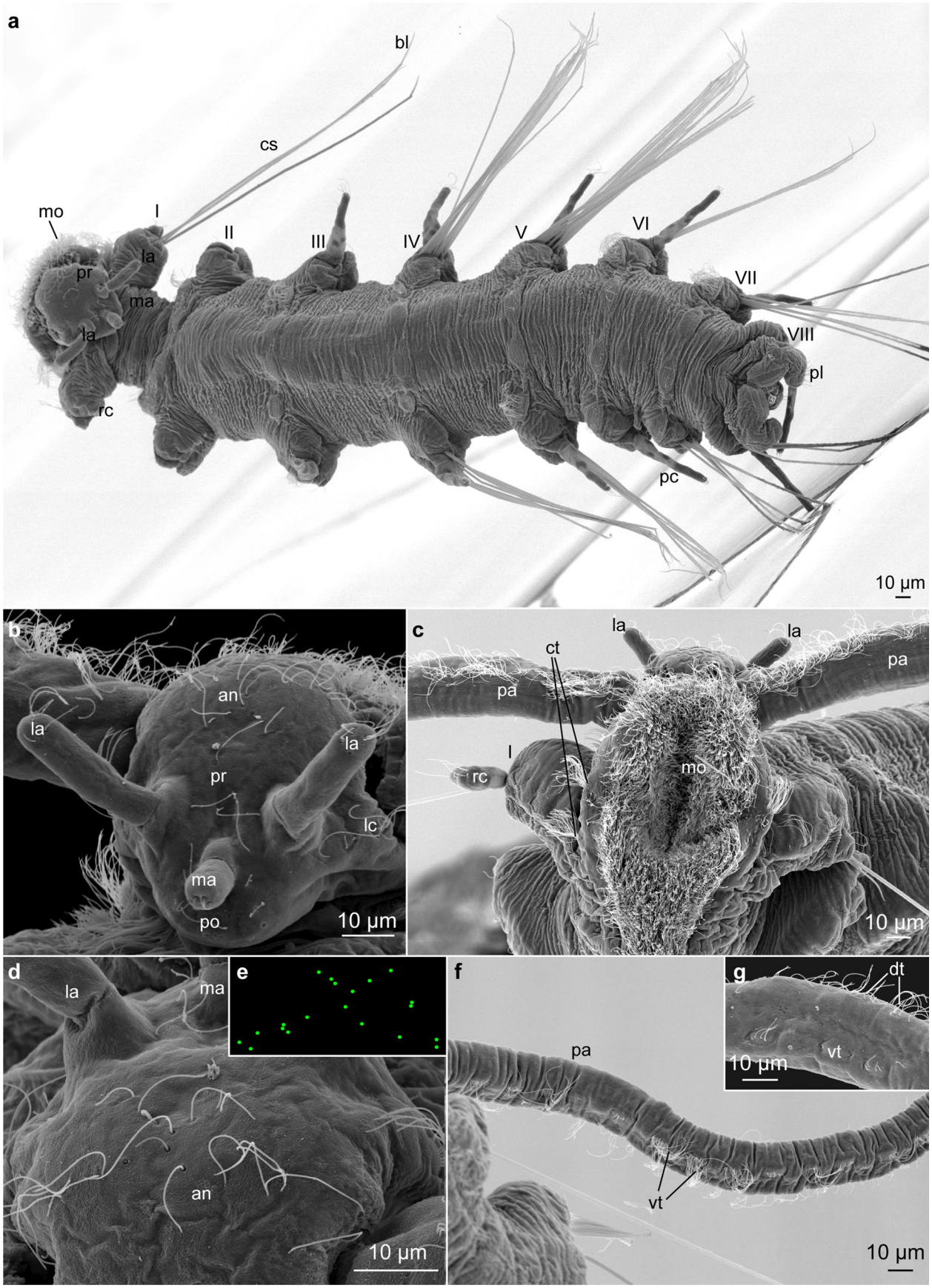
a
bl
cs
mo
I
II
III
IV
V
VI
VII
VIII
la
pr
ma
la
rc
pl
pc
10 μm
b
an
la
la
pr
lc
ma
po
10 μm
c
la
la
ct
pa
pa
I
rc
mo
10 μm
d
la
ma
an
10 μm
e
f
pa
vt
10 μm
g
dt
vt
10 μm

◀ **Fig. 2** *Speleonerilla calypso* sp. n. Scanning electron micrographs of **a** entire specimen (both palps lost) in dorsal view; **b** prostomium with three dorsal antennae, dorsal view; **c** peristomium, ventral view; **d** prostomium with anterior field of sensory cilia (as), antero-dorsal view; **e** mapping of as; **f** dorsal view of palp; **g** detail of palp. an, anterior field of sensory cilia; bl, chaetal blade; cs, chaetal shaft; ct, cilary tufts; dt, dorsal ciliary tufts; la, lateral antenna; lc, prostomial lateral ciliation; ma, median antenna; mo, mouth; pa, palps; pc, parapodial cirri; pl, pydigial lobe; po, posterior field of sensory cilia; pr, prostomium; rc, rudimental cirrus; vt, ventral ciliary tufts; I–VIII, segments I–VIII

15–20 m depth, 26.3755–77.1041, December 2008 (Coll: B.C. Gonzalez & T.M. Iliffe). Paratypes: 20 from the same collecting trip as holotype with nine specimens (NHMD-218143) placed on the same SEM stub as holotype, one specimen placed on separate SEM stub (NHMD-218144), nine specimens mounted in glycerol as permanent whole mounts (NHMD-218145–NHMD-218153); two additional whole mounts (for CLSM, NHMD-21854, NHMD-21855) from the same locality as holotype but collected 11 March 2017 (Coll: T.M. Iliffe, L. Ballou & J. Olesen). ZooBank number: urn:lsid:zoobank.org: act:DA703609-D0F9-4FDF-B933-AFE28333E89E.

Diagnosis *Speleonerilla* with eight segments. Parapodium with up to 15 compound chaetae per fascicle. Rudimental cirri on segment I. Parapodial interramal cirri on segments III–VIII. Neuropodial chaetal lobes on segments II–VIII. Three pairs of nephridia opening in segments III, IV, and V. Hermaphroditic with one pair of spermioducts and one pair of oviducts opening in segments VII and VIII, respectively.

Etymology The species is named after the dance calypso, which originated in Trinidad & Tobago and later spread to other Caribbean Islands, including the Bahamas.

Description All measurements from holotype, numbers given in parentheses from paratypes; most measures are from SEM preparations (see Table 2). Body with eight chaetigerous segments (Fig. 1a and 2a), 501 μm long (464–895 μm, $n = 17$), 167 μm wide including parapodia (142–298 μm, $n = 17$), 126 μm excluding parapodia (86–218 μm, $n = 17$). Segments I–IV equal in length, segments V–VIII decreasing in length posteriorly, pygidium shortest, 24 μm (16–36 μm, $n = 9$).

Prostomium short and rounded (Figs. 1a and 2a), 60 μm long (26–60 μm, $n = 13$), 43 μm wide (43–110 μm, $n = 10$), with two thread-like ventrolateral palps (Figs. 1a and 2f) and three short antennae (Fig. 2a–c). Palps maximum 425 μm long (400–620 μm, $n = 9$), lateral antennae maximum 29 μm long (26–35 μm, $n = 10$), median antenna 17 μm long (16–22 μm, $n = 3$). Eyes absent. Nuchal organs appear as round elevated bulges on lateral sides of prostomium situated between palps and parapodia of segment I (not shown). Large glandular cells line midgut wall (Fig. 1d).

Segment I with uniramous parapodia, 36 μm long (24–50 μm, $n = 12$), segments II–VIII with biramous parapodia, maximum 34 μm long (24–52 μm, $n = 10$) (Figs. 1a and 2a). Rudimental parapodial cirri (Fig. 2c) on segment I, 23 μm long (7–23 μm, $n = 7$). Interramal parapodial cirri on segments III–VIII (Figs. 1a, 2a, and 3d), maximum 60 μm long (43–77 μm, $n = 14$); parapodial cirri cylindrical and slightly increasing in length toward pygidium (Fig. 2a). Parapodial cirri with glandular oval cells throughout (Fig. 1b). Neuropodial chaetal lobe on segments II–VIII (Fig. 3b), absent on segment I.

Pygidium short, with two lobes (Figs. 1a, 2a, and 3f), 36 μm long (19–52 μm, $n = 14$), each with two projections and dense ciliation (Fig. 3f). Pygidial cirri not observed, but two scars visible with SEM (Fig. 3f).

All chaetae compound (Figs. 1c and 2a); shafts with small pointed distal extension, 2 μm long (2–3 μm, $n = 5$). Alternating pocket-like structures projecting outwards along shaft margins. Blades lacking ornamentation. Segment I, with 14 chaetae per fascicle (10–14, $n = 6$); segments II–VIII each with dorsal and ventral fascicles of up to 15 (9–15, $n = 3$) and up to 14 chaetae (7–14, $n = 4$). Shaft maximum 137 μm long (137–189 μm, $n = 10$), blade maximum 24 μm long (19–41 μm, $n = 10$); total length maximum 161 μm (161–216 μm, $n = 11$).

Prostomium with paired lateral ciliary bands extending laterally between bases of each lateral antenna and insertion of palp (Fig. 2b). Prostomium with anterior field of sensory cilia arranged in an X pattern anterior of the antennae (Fig. 2d, e); posterior to the median antenna with field of several individual cilia (Fig. 2b). Two dense tufts of cilia present on each ventrolateral side of ventral mouth ciliary field (Fig. 2c).

Palps with ventral and frontal longitudinal ciliary bands extending from the insertion to the tip of the palp (Fig. 2c, f). Palp ventral ciliary band consists of tufts with > 25 cilia, up to 18 μm long (not observed in holotype; $n = 1$) and spaced 8 μm apart (Fig. 2f). Palp frontal ciliary band consists of individually arranged, presumably sensory, cilia. Few individual cilia (~ 4), 7 μm long, are found scattered between both bands (Fig. 2g).

Dorsal body ciliation consisting of transverse rows of ciliary tufts (up to four) on segments I–VIII at the level of parapodia (Fig. 3c). Each tuft with more than 50 motile cilia. Ventral body surface with dense ciliation, consisting of mouth ciliation (Fig. 2c), a narrow midventral ciliary band extending from mouth to anus,

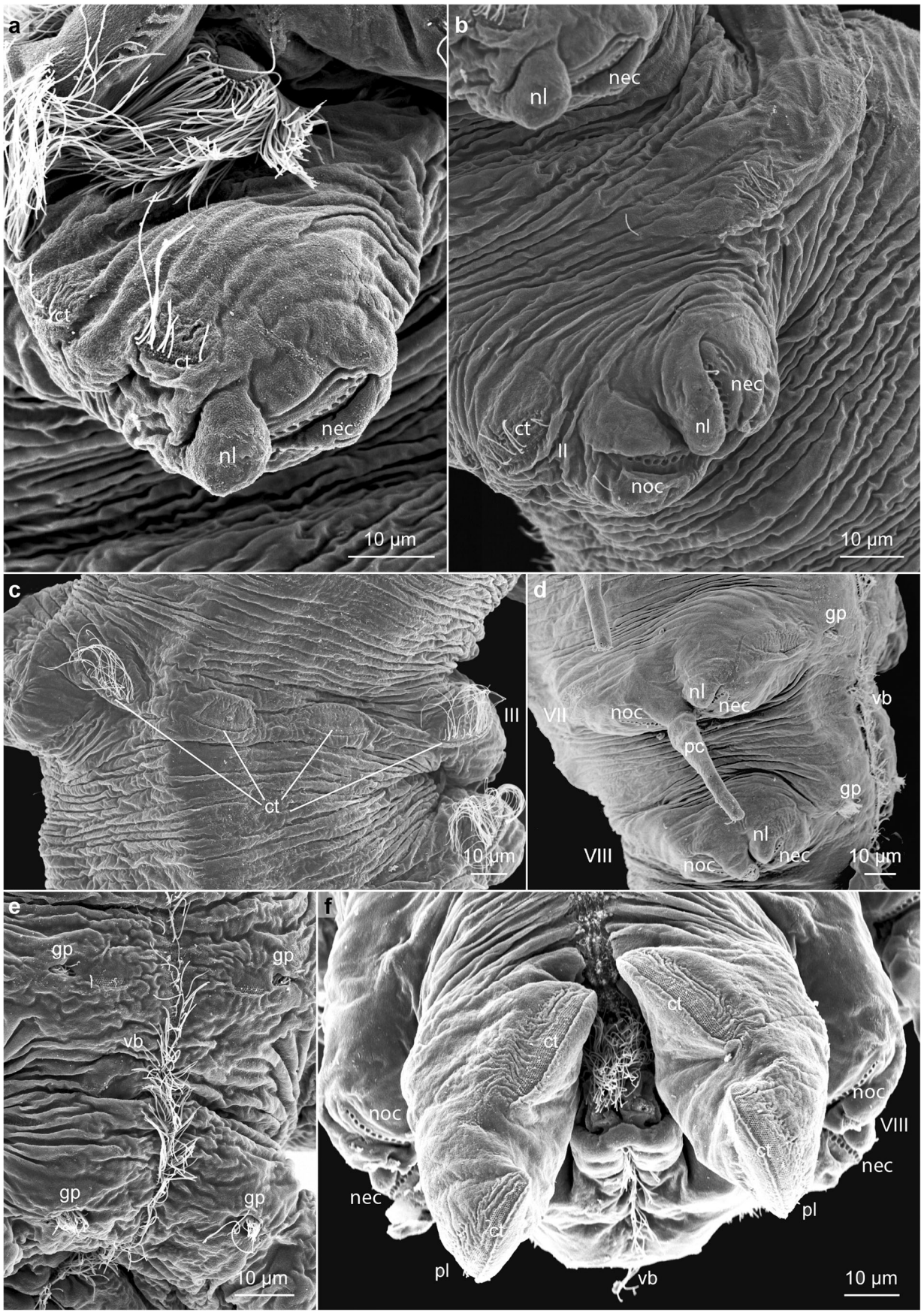
a
ct
ct
nec
nl
10 µm
b
nec
nl
nec
nl
ct
II
noc
10 µm
c
III
ct
10 µm
d
gp
nl
nec
vb
VII
noc
pc
gp
nl
VIII
noc
nec
10 µm
e
gp
gp
vb
gp
gp
10 µm
f
ct
ct
noc
VIII
ct
nec
nec
pl
ct
pl
vb
10 µm

◀ **Fig. 3** *Speleonerilla calypso* sp. n. Scanning electron micrographs of **a** neuropodial chateal lobe on segment I, ventral view (all chaetae lost); **b** neuropodial chaetal lobe on segment II in dorsolateral view; **c** four dorsal ciliary tufts on segment III; **d** segments VII–VIII with gonopores and parapodial cirrus, lateral view; **e** segments VII–VIII with ventral ciliary band and ventral gonopores; **f** posterior body with terminal pygidigial lobes and ciliary tufts. ct, cilary tufts; gp, gonopore; nec, neurochaetae (chaetal holes, since chaetae are missing); nl, neuropodial chaetal lobe; noc, notopodial chaetae (chaetal holes, since chaetae are missing); pc, parapodial cirri; pl, pydigial lobe; vb, ventral ciliary band; II–VIII, segments II–VIII

continuing dorsally atop pygidium, and transverse rows of four–eight ciliary tufts at each segment (Fig. 3b, d, e, Table 2). Additional single ventral ciliary tufts on each ventrolateral side, between prostomium and segment I (Fig. 2c) and between segments I and II (not shown) (Table 2).

Hermaphroditic. Nephridia and gonoducts investigated using CLSM (Fig. 1e). Three pairs of segmental nephridia, running dorsoventrally, parallel to ventral nerve cord, nephridiopores opening ventrally in segments III, IV, and V near segment borders. Enteronephridia not observed. One pair of relatively straight spermioducts, opening in segment VII and one pair of straight oviducts opening in segment VIII. Two pairs of gonopores also observed with SEM (Fig. 3d, e).

Distribution and habitat Cherokee Road Extension Blue Hole "Magical Sinkhole," Abaco Island, Bahamas. Inland anchialine blue hole with depths over 100 m. Halocline at 15–20 m with strong hydrogen sulfide layer (Gonzalez et al. 2011).

Remarks *Speleonerilla calypso* sp. n. differs from *S. saltatrix* (Worsaae et al. 2004; Worsaae and Müller 2004) in the presence of one additional pair of nephridia opening on segment V, rudimental cirri on segment I, and more abundant and longer neurochaetae (Table 3). This species most closely resembles *S. salsa* sp. n. but differs by a longer maximum length, presence of rudimental cirri on segment I, and slightly more and longer chaetae. Genetic distances to the other species of the genus are summarized in Table 4.

Speleonerilla salsa sp. n.

Figures 4, 5, and 6; Tables 1, 2, 3, and 4

Type material Holotype (NHMD-218173) on SEM stub, 411 μm long, Casimba El Brinco, Cuba, water column, 20–30 m, 22.076/− 81.056, November 2014 (Coll. A. Martínez & B.C. Gonzalez). Paratypes: three specimens (NHMD-218174) on the same SEM stub as holotype, and eight specimens as whole mounts (in glycerol) (NHMD-218175–NHMD-218182), the same collecting trip as holotype. One specimen lost in the process. ZooBank number: urn:lsid:zoobank.org: act:33B37943-4F2F-44C6-A545-8DC97980E52E.

Diagnosis *Speleonerilla* with eight segments. Parapodium with up to 13 compound chaetae per fascicle. Parapodial interramal cirri on segments III–VIII. No rudimental cirri on segment I. Neuropodial chaetal lobes from segments I–VIII. Three pairs of segmental nephridia opening in segments III, IV, and V. Hermaphroditic with one pair of spermioducts opening in segment VII, and one pair of oviducts in segment VIII.

Etymology The species is named after the dance salsa, the musical roots of which lie in Eastern Cuba.

Description All measurements from holotype, numbers given in parentheses from paratypes. Most measurements taken from SEM preparations (see Table 2). Body with eight chaetigerous segments (Figs. 4a and 5a, b), 411 μm long (411–733 μm, $n = 12$), 158 μm wide including parapodia (125–221 μm, $n = 12$), 117 μm excluding parapodia (116–121 μm, $n = 4$). Segments I–IV longest, segments V–VIII decreasing in length posteriorly, pygidium shortest, 28 μm (8–29 μm, $n = 11$).

Prostomium short and rounded (Figs. 4a and 5e), 36 μm long (33–76 μm, $n = 10$), 47 μm wide (47–130 μm, $n = 10$), with two thread-like ventrolateral palps (Fig. 5c) and three short antennae (Figs. 4a, b and 5e). Palps, maximum 373 μm long (absent on holotype; $n = 1$); lateral antennae, maximum 30 μm long (21–39 μm, $n = 7$), median antenna, broken in holotype (17–18 μm, $n = 2$). Eyes absent. Nuchal organs appear as round elevated bulges on each lateral side of prostomium, situated between palps and parapodia of segment I (Figs. 5e and 6a).

Parapodia on segment I, uniramous (15–41 μm, $n = 8$, measurements from paratypes only), parapodia on segments II–VIII, biramous, 24 μm long (14–34 μm, $n = 7$). Interramal parapodial cirri on segments III–VIII (Fig. 5a), maximum 48 μm long (34–64 μm, $n = 7$); parapodial cirri cylindrical and slightly increasing in length toward pygidium (Fig. 5a, b). Neuropodial chaetal lobe on segments I–VIII (Figs. 5b and 6a).

Pygidium short, with two relatively long pygidial lobes (Figs. 4a, 5a, b, and 6b, c), 48 μm long (19–48 μm, $n = 7$), each with two projections and dense ciliation (Fig. 6b, c). Pygidial cirri not observed, scars visible with SEM (Fig. 6c).

Table 2 Measurements and morphometric characters of *Speleonerilla* spp.

	Speleonerilla calypso sp. n.					*Speleonerilla salsa* sp. n.					*Speleonerilla isa* sp. n.				
	Holotype	Min.	Max.	Average	*n*	Holotype	Min.	Max.	Average	*n*	Holotype	Min.	Max.	Average	*n*
Total L	*501*	*464*	895	697	17	*411*	*411*	733	610	12	*391*	329	580	432	6
Max. W incl. para.	*167*	*142*	298	206	17	*158*	*125*	221	164	12	*109*	*109*	186	141	6
Max. W excl. para.	*126*	*86*	218	159	17	*117*	116	121	119	4	*73*	*73*	140	110	5
Prostomium L	*60*	26	*60*	45	13	*36*	*36*	76	50	10	*40*	26	50	40	4
Prostomium W	*43*	*43*	110	72	13	*47*	47	130	96	10	*55*	37	64	51	4
Max. L palps	*425*	*400*	620	509	9	?	*373*	373	373	1	*253*	*253*	380	317	3
L median ant.	*17*	*16*	*22*	18	3	?	*17*	18	18	2	?	55	55	55	1
Max. L lat. ant.	*29*	21	37	30	10	*30*	21	39	31	7	?	46	46	46	1
L segm. 1	*45*	*45*	157	90	11	?	*72*	196	118	9	*41*	*41*	101	71	2
L segm. 2	*43*	*43*	148	101	12	*42*	*42*	115	92	10	*50*	*50*	71	61	2
L segm. 3	*59*	*59*	133	98	12	*51*	*51*	142	88	10	*42*	*42*	56	49	2
L segm. 4	*76*	*49*	125	89	12	*48*	*48*	107	82	11	*42*	*42*	56	49	2
L segm. 5	*52*	*44*	101	74	12	*44*	*44*	104	65	11	*35*	*35*	48	42	2
L segm. 6	*56*	*33*	105	65	12	*34*	*34*	75	50	11	*34*	*34*	47	41	2
L segm. 7	*35*	*33*	57	46	12	*39*	18	70	41	11	*29*	*29*	41	35	2
L segm. 8	*26*	*26*	47	38	12	*33*	15	40	27	11	*23*	*23*	31	27	2
L segm. 9	na	na	na	na		na	na	na	na		*16*	*16*	25	21	2
L pygidium	*24*	16	36	25	12	*28*	8	29	19	11	*24*	*24*	28	26	2
Max. L para. segm.1	*36*	24	50	37	12	?	15	41	25	8	*19*	*19*	23	21	2
Max. L other para.	*34*	24	*52*	35	13	*24*	*14*	34	23	7	*18*	14	27	20	4
Max. L cirri segm.1	*23*	7	23	10	7	?	?	?	?		*7*	*7*	8	8	2
Max. L para. cirri	*60*	*43*	77	62	14	*48*	34	*64*	45	7	*43*	21	92	48	4
Max. L pyg. lobes	*36*	19	52	40	14	*48*	19	*48*	32	7	*11*	*11*	17	14	4
Chaetae															
Max. # segm.1	*14*	10	*14*	10	6	*13*	*13*	*13*	13	2	*11*	*11*	12	12	3
Max. # notochaetae	?	9	*15*	11	3	10	9	10	10	2	*11*	7	*11*	9	3
Max. # neurochaetae	*14*	7	*14*	11	4	*13*	*13*	*13*	13	2	*7*	*7*	9	8	3
Max. total L	*161*	*161*	*216*	191	11	*122*	59	184	125	9	*122*	120	131	124	3
Max. L shaft	*137*	*137*	*189*	165	10	*86*	70	105	87	6	*113*	84	*113*	100	3
Max. L dist. ext. shaft	*2*	*2*	*3*	3	5	*3*	*2*	*4*	3	4	*3*	*3*	3	3	2
Max. L blade	*24*	19	*41*	25	10	*26*	*15*	34	26	5	*20*	*20*	36	25	3
Dorsal ciliary tufts															
# segm. 1	?	?	?	?	2	?	?	?	?	2	*2*	*2*	*2*	*2*	1
# segm. 2	*4*	*4*	*4*	*4*	2	*4*	*4*	*4*	*4*	2	*6*	*6*	*6*	*6*	1

Table 2 (continued)

	Speleonerilla calypso sp. n.					*Speleonerilla salsa* sp. n.					*Speleonerilla isa* sp. n.				
	Holotype	Min.	Max.	Average	*n*	Holotype	Min.	Max.	Average	*n*	Holotype	Min.	Max.	Average	*n*
# segm. 3	*4*	*4*	*4*	*4*	2	*4*	*4*	*4*	*4*	2	*6*	*6*	*6*	*6*	1
# segm. 4	*4*	*4*	*4*	*4*	2	*4*	*4*	*4*	*4*	2	*6*	*6*	*6*	*6*	1
# segm. 5	*4*	*4*	*4*	*4*	2	*4*	*4*	*4*	*4*	2	*6*	*6*	*6*	*6*	1
# segm. 6	*4*	*4*	*4*	*4*	2	*4*	*4*	*4*	*4*	2	*6*	*6*	*6*	*6*	1
# segm. 7	*4*	*4*	*4*	*4*	2	*2*	*2*	*4*	*2, 4*	2	*6*	*6*	*6*	*6*	1
# segm. 8	*2*	*2*	*2*	*2*	2	*2*	*2*	*2*	*2*	2	*4*	*4*	*4*	*4*	1
# segm. 9	na	na	na	na		na	na	na	na		*2*	*2*	*2*	*2*	1
Ventral ciliary tufts															
# segm. 1	*8*	*8*	*8*	*8*	2	*8*	*8*	*8*	*8*	2	*8*	*8*	*8*	*8*	1
# between segm. 1&2	*2*	*2*	*2*	*2*	2	*2*	*2*	*2*	*2*	2	*4*	*4*	*4*	*4*	1
# segm. 2	*8*	*8*	*8*	*8*	2	*8*	*8*	*8*	*8*	2	*8*	*8*	*8*	*8*	1
# segm. 3	*8*	*8*	*8*	*8*	2	*8*	*8*	*8*	*8*	2	*8*	*8*	*8*	*8*	1
# segm. 4	*6*	*6*	*6*	*6*	2	*6*	*6*	*6*	*6*	2	*8*	*8*	*8*	*8*	1
# segm. 5	*6*	*6*	*6*	*6*	2	*6*	*6*	*6*	*6*	2	*6*	*6*	*6*	*6*	1
# segm. 6	*6*	*6*	*6*	*6*	2	*6*	*6*	*6*	*6*	2	*4*	*4*	*4*	*4*	1
# segm. 7	*4*	*4*	*4*	*4*	2	*4*	*4*	*4*	*4*	2	*4*	*4*	*4*	*4*	1
# segm. 8	?	*2*	*4*	*2, 4*	2	*2*	*2*	*4*	*2, 4*	2	*4*	*4*	*4*	*4*	1
# segm. 9	na	na	na	na		na	na	na	na		?	?	?	?	1

Measurements in italics based on SEM specimens (rather than whole mounts). Measurements are given in micrometers but have an error margin of a few micrometers

ant., antenna; *dist.*, distal; *excl.*, exclusive; *ext.*, extension; *incl.*, inclusive; *L*, length; *lat.*, lateral; *min.*, minimum; *max.*, maximum; *na*, not applicable; *para*, parapodia; *pyg*, pygidium; *segm.*, segment; *W.*, width; #, number

Table 3 Comparison of the main characteristics of *Speleonerilla* spp.

	Max length	Segm. #	Rud. parapodial cirri, segm. I	Neur. chaetal lobes	Parapodial cirri on segm.	Max. # ventral ciliary tufts on segm. VI, VII, VIII	Max. # dorsal ciliary tufts on segm. VI, VII, VIII	Nephridia opening in segm.	Spemioduct opening in segm.	Max. length chaetae	Max. number chaetae, segm. I	Max. number chaetae: noto./ neur.
Speleonerilla saltatrix (Bermuda)	985	8	–	I–VIII	III–VIII	6, 6, 4	4, 4, 2	3, 4	7	145	13	10/10
Speleonerilla calypso (Bahamas)	895	8	+	II–VIII	III–VIII	6, 4, 4	4, 4, 2	3, 4, 5	7	216	14	15/14
Speleonerilla salsa (South Cuba)	733	8	–	I–VIII	III–VIII	6, 4, 4	4, 4, 2	3, 4, 5	7	184	13	10/13
Speleonerilla isa (Lanzarote)	580	9	+	IV–IX	II–IX	4, 4, 4	6, 6, 4	3, 4, 5	6, 7**	131	12	11/9
Speleonerilla sp. A (Northeast Cuba)	430*	8	?	?	III–VIII	?	?	?	7	117	?	?
Speleonerilla sp. B (Yucatán, México)	659	8	?	?	III–VIII	?	?	3, 4	7	145	?	?

Measurements done on specimens fixed in aldehyde, except for *specimen fixed in 99% ethanol. **, open midventrally (versus ventrolaterally). All measurements in micrometers

Max., maximum; *neur.*, neuropodial; *noto.*, notopodial; *segm.*, segment; *Rud.*, rudimental

All chaetae compound, straight (Figs. 5b and 6d); shafts with small pointed distal extension (Fig. 6d), 3 μm (2–4 μm, $n = 4$). Alternating pocket-like structure projecting outwards along shaft margins. Blades without ornamentation (Fig. 6e). Segment I with up to 13 chaetae per fascicle ($n = 2$); segments II–VIII with ventral fascicles of up to 13 neuropodial chaetae ($n = 2$) and dorsal fascicle with up to 10 notochaetae ($n = 2$). Shaft maximum 86 μm long (70–105 μm, $n = 6$), blade maximum 26 μm long (15–34 μm, $n = 5$); total length maximum 122 μm (59–184 μm, $n = 9$).

'Prostomial ciliation comprise two ciliated areas, anterior and posterior to median antenna, respectively, consisting of individual cilia, and paired lateral ciliary bands extending from each lateral antenna to the insertion of the palps (Fig. 5e).

Palps with ventral and frontal longitudinal bands extending from the insertion to the tip of the palp (Fig. 5c). Palp ventral ciliary band consists of tufts of more than 50 cilia, up to 17 μm long (not observed in holotype; $n = 1$) and spaced ca. 17 μm apart (Fig. 5c, d). Palp frontal ciliary band consists of individually arranged, presumably sensory, cilia. Few individual cilia are found scattered between both bands (Fig. 5d).

Dorsal transverse rows of up to four ciliary tufts across segments II–VIII at the level of the parapodia; each tuft with more than 50 motile cilia. Ventral body surface with dense ciliation, consisting of mouth ciliation, a midventral ciliary band extending to dorsal anus on pygidium (Fig. 6c), and transverse rows of four–eight ciliary tufts at the level of parapodia (see Table 2). A single additional ventral ciliary tuft present between prostomium and segment I and between segments I and II, on each ventrolateral side (Fig. 6a).

Hermaphroditic. Nephridia and gonoducts investigated using CLSM (Fig. 4d). Three pairs of segmental nephridia running dorsoventrally, parallel to ventral nerve cord, nephridiopores opening ventrally in segments III, IV, and V near segment borders. Enteronephridia not observed. One pair of spermioducts, relatively straight, opening in segment VII; one pair of gonoducts opening in segment VIII.

Table 4 *Speleonerilla* spp. distance matrix of all genes sequenced

18S	1	*Speleonerilla salsa*					
	2	*Speleonerilla saltatrix*	0.997				
	3	*Speleonerilla calypso*	0.992	0.992			
	4	*Speleonerilla* sp. B	0.992	0.994	0.994		
	5	*Speleonerilla* sp. A	0.989	0.989	0.985	0.988	
	6	*Speleonerilla isa*	0.960	0.961	0.961	0.958	0.956
28S	1	*Speleonerilla salsa*					
	2	*Speleonerilla saltatrix*	0.932				
	3	*Speleonerilla calypso*	0.875	0.897			
	4	*Speleonerilla* sp. B	0.864	0.877	0.896		
	5	*Speleonerilla* sp. A	0.826	0.839	0.856	0.874	
	6	*Speleonerilla isa*	0.831	0.834	0.833	0.850	0.818
COI	1	*Speleonerilla salsa*					
	2	*Speleonerilla saltatrix*	0.536				
	3	*Speleonerilla calypso*	0.482	0.602			
	4	*Speleonerilla* sp. B	0.476	0.576	0.600		
	5	*Speleonerilla* sp. A	0.482	0.569	0.582	0.554	
	6	*Speleonerilla isa*	0.441	0.575	0.595	0.546	0.535
H3	1	*Speleonerilla salsa*					
	2	*Speleonerilla calypso*	0.924				
	3	*Speleonerilla* sp. A	0.924	0.903			
	4	*Speleonerilla isa*	0.882	0.873	0.877		

Distribution and habitat Casimba El Brinco, Ciénaga de Zapata, Matanzas, South Cuba. Anchialine limestone cave, with a halocline at 5–8 m depth and a total depth of 80 m.

Remarks *Speleonerilla salsa* sp. n. differs from *S. saltatrix* in having one additional pair of nephridia opening in segment V and more and longer neurochaetae (Table 3). It most closely resembles *S. calypso* sp. n. but differs by a shorter maximum length, absence of rudimental cirri on segment I, and by having fewer, shorter chaetae. Genetic distances to the other species of the genus are summarized in Table 4.

Speleonerilla isa sp. n.

Figures 7, 8, and 9; Tables 1, 2, 3, and 4 Type material

Holotype (NHMD-218167) on SEM stub, 391 μm long, Túnel de la Atlántida, Lanzarote, water column, 2–20 m, 29.157051/− 13.430459, October 2011 (Coll. A. Martínez, E. Domínguez, L. E. Cañadas, B. C. Gonzalez, K. Worsaae). Paratypes: five specimens as permanent whole mounts (in glycerol, NHMD-218168–NHMD-218172)), the same collecting site as holotype, collected October 2011 and April 2014 (Coll. A. Martínez, E. Domínguez, L. E. Cañadas, B. C. Gonzalez, K. Worsaae). ZooBank number: urn:lsid:zoobank.org: act:DAE63780-D1B2-4EF3-8F38-1CED31ADEFB7.

Diagnosis *Speleonerilla* with nine segments. Parapodia with up to 12 compound chaetae in each fascicle. Parapodia on segments II–IX, well-developed and biramous, up to 11 compound chaetae per fascicle. Rudimental cirri present on segment I, parapodial cirri from segments II–IX. Neuropodial chaetal lobes from segments IV–IX. Pygidium with densely ciliated, paired pygidial lobes and long filiform pygidial cirri. Dorsal transverse rows of up to six tufts per segment. Three pairs of nephridia opening in segments III, IV, and V. Hermaphroditic with two pairs of long, angled spermioducts opening in segments VI and VII, and one

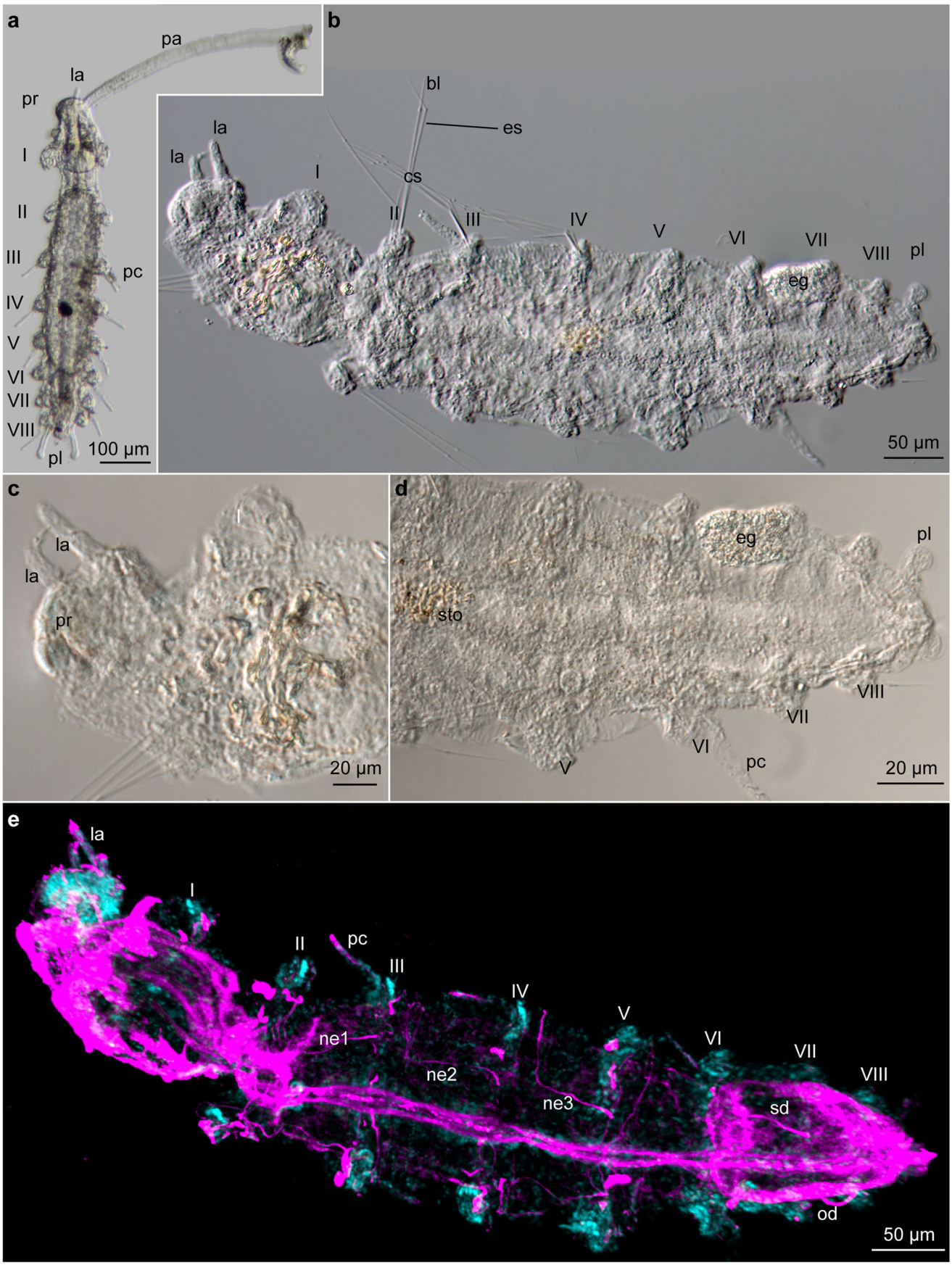
a
pa
la
pr
I
II
III
pc
IV
V
VI
VII
VIII
pl
100 µm
b
bl
es
la
la
I
cs
II
III
IV
V
VI
VII
VIII
pl
eg
50 µm
c
la
la
pr
I
20 µm
d
eg
pl
sto
VIII
VII
VI
pc
V
20 µm
e
la
I
II
pc
III
IV
V
VI
VII
VIII
ne1
ne2
ne3
sd
od
50 µm

◀ **Fig. 4** *Speleonerilla salsa* sp. n. Light microscopy images of **a** live specimen with one palp; **b** whole specimen (both palps lost) in ventral view; **c** detail of prostomium with two lateral antennae; **d** segments V–VIII with egg; **e** maximum intensity projection of CLSM image stack showing segmentally arranged nephridia, oviducts, and spermioducts in ventrolateral view (pink—acetylated α-tubulin-like immunoreactivity, cyan—DAPI). bl, chaetal blade; cs, chaetal shaft; eg, egg; es, extension shaft; la, lateral antenna; ne1–3, segmental nephridia; od, oviduct; pa, palp; pc, parapodial cirri; pl, pydigial lobe; pr, prostomium; sd, spermioduct; I–VIII, segments I–VIII

pair of oviducts opening in segment VIII. All gonopores placed ventromedian (rather than ventrolateral).

Etymology The species is named after the Canarian traditional folk dance "isa" from Lanzarote.

Description All measurements from holotype, numbers given in parentheses from paratypes. Most measurements taken from SEM preparations (see Table 2). Body with nine chaetigerous segments (Figs. 7a and 8a), 391 μm long (329–580 μm, $n = 6$), 109 μm wide including parapodia (109–186 μm, $n = 6$), 73 μm wide excluding parapodia (73–140 μm, $n = 5$). Segment decreasing in length posteriorly, pygidium shortest, 24 μm (24–28 μm, $n = 2$).

Prostomium short and rounded (Fig. 7a, b), 40 μm long (26–50 μm, $n = 4$), 55 μm wide (37–64 μm, $n = 4$), with two thread-like ventrolateral palps and three short antennae. Palps maximum 253 μm long (229–380 μm, $n = 3$) (Fig. 7a); lateral antennae maximum 46 μm long (absent in holotype; $n = 1$), median antenna 55 μm (absent in holotype; $n = 1$) (Fig. 8a, b). Eyes absent. Nuchal organs paired, appear as a round elevated bulge on each lateral side of prostomium, between palps and parapodia of segment I (Fig. 8a).

Parapodia on segment I, uniramous, 19 μm long (19–23 μm, $n = 2$), parapodia on segments II–IX, maximum 18 μm long (14–27 μm, $n = 4$). Rudimental parapodial cirri on segment I (Fig. 8a, e–g), 7 μm (7–8 μm, $n = 2$). Interramal parapodial cirri on segments II–IX maximum 43 μm long (21–92 μm, $n = 4$); parapodial cirri cylindrical and slightly increasing in length toward pygidium (Fig. 8a). Parapodial cirri with glandular oval cells throughout (Fig. 7c). Neuropodial chaetal lobe, segments IV–IX.

Pygidium short, with two pygidial lobes (Fig. 7a), 11 μm long (11–17 μm, $n = 4$), each with two projections and dense ciliation. Long filiform pygidial cirri observed on live specimen, scars visible with SEM.

All chaetae compound, straight (Fig. 8a); shaft with small pointed distal extension (Fig. 9c), 3 μm ($n = 2$). Alternating pocket-like structures projecting outwards along shaft margins. Blades lacking ornamentation. Segment I with maximum 12 chaetae per fascicle ($n = 3$); segments II–IX, each with dorsal and ventral fascicles of maximum 11 and 9 chaetae ($n = 1$). Shaft maximum 113 μm long (84–113 μm, $n = 3$), blade maximum 20 μm long (20–36 μm, $n = 3$); total length maximum 122 μm (120–131 μm, $n = 4$).

Prostomium with paired lateral ciliary bands extending from each lateral antenna to insertion of palps. Prostomial anterior field of sensory cilia with transverse row of individual sensory cilia, dorsal to lateral antennae, and a secondary curved row above them (Fig. 8c, d). Prostomial posterior field of sensory cilia posterior of median antenna with several individual cilia (Fig. 8b–d). Two lateral ciliary tufts present on each lateral side of prostomium (Fig. 8b).

Palps with ventral and frontal longitudinal bands extending from insertion to tip of palp. Palp ventral ciliary band consists of tufts of more than 30 cilia, up to 9 μm long (not observed in holotype; $n = 1$). Palp frontal ciliary band consists of individually arranged, presumably sensory cilia. Few individual cilia are found scattered between both bands.

Dorsal transverse rows at the level of parapodia, each with up to six ciliary tufts (see Table 2) (Fig. 9a); each tuft with more than 50 motile cilia. Ventral mouth area heavily ciliated, continuing into narrow midventral ciliary band, extending to anus, and dorsally atop pygidium (Figs. 8a and 9b). Ventral rows of up to eight ciliary tufts, aligned with parapodia (Fig. 8f). A single additional ciliary tuft present on each ventrolateral side, between prostomium and segment I (not shown) and between segments I and II (Fig. 8g).

Hermaphroditic. Nephridia and gonoducts investigated using CLSM (Fig. 7d). Three pairs of segmental nephridia, running dorsoventrally, parallel to ventral nerve cord, opening ventrally on segments III, IV, and V. Enteronephridia not observed. Two pairs of spermioducts and one pair of oviducts, initiating dorsally, perpendicular to ventral nerve cord, bending 110° toward ventral midline, where they open on segments VI, VII, and VIII.

Distribution and habitat Túnel de la Atlántida, La Corona lava tube, Lanzarote, Canary Islands. Lava tube with no conspicuous halocline, 2–15 m deep, almost no sediment. Mainly collected at entrance pool of Túnel de la Atlántida (Martínez et al. 2016).

Remarks *Speleonerilla isa* sp. n. differs markedly from the Caribbean species of *Speleonerilla* by having nine segments (versus eight), two pairs (versus one) of spermioducts that open in a common midventral

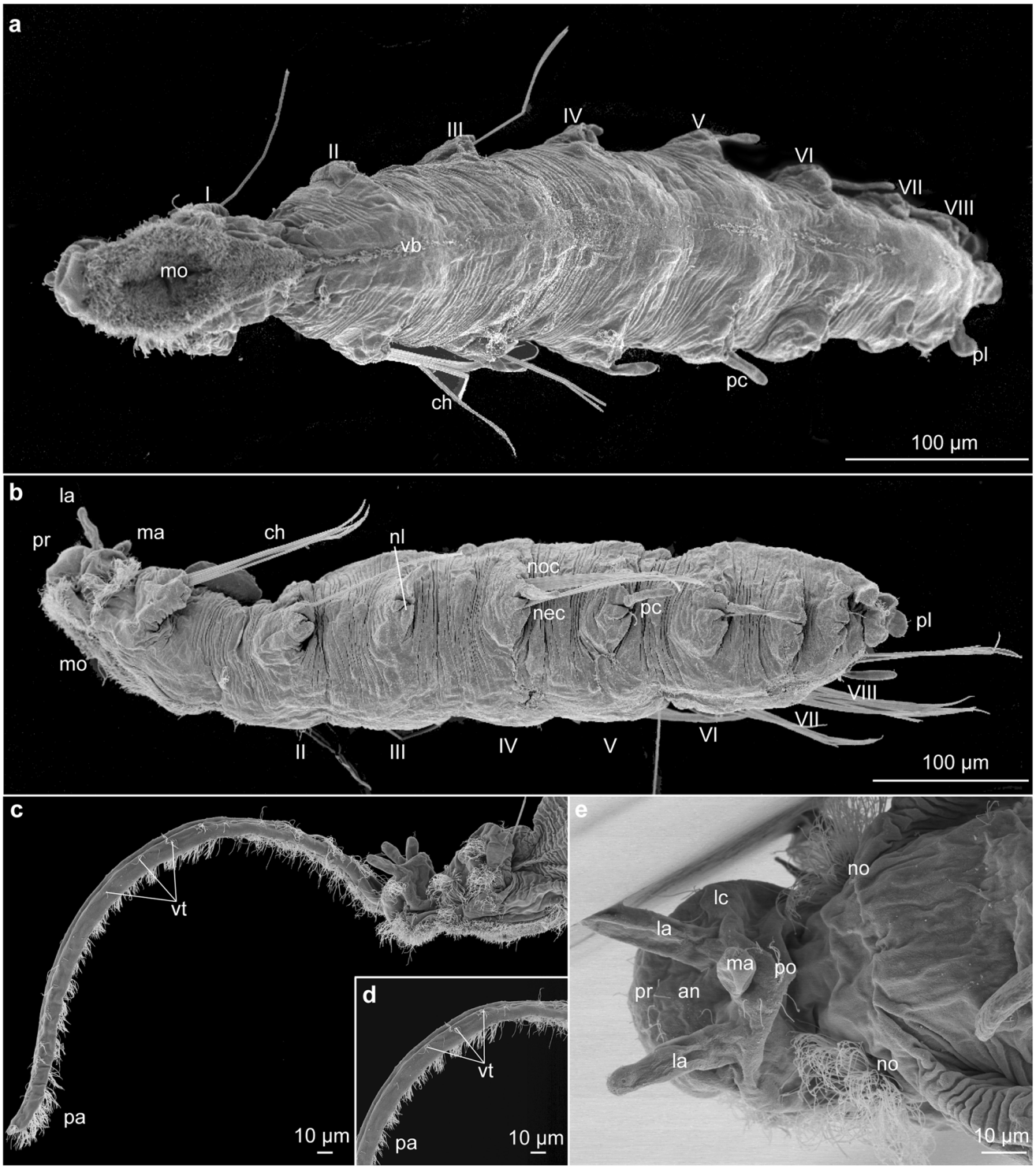

Fig. 5 *Speleonerilla salsa* sp. n. Scanning electron micrographs of **a** whole specimen (both palps lost) in ventral view; **b** whole specimen in lateral view (dorsal side up); **c** prostomium with palp in lateral view; **d** closer view of palp; **e** dorsal view of prosotomium and nuchal organs. an, anterior field of sensory cilia; ch, chaetae; la, lateral antenna; lc, prostomial lateral ciliation; ma, median antenna; mo, mouth; nec, neurochaetae (chaetal holes, since chaetae are missing); nl, neuropodial chaetal lobe; no, nuchal organs; noc, notopodial chaetae (chaetal holes, since chaetae are missing); pa, palps; pc, parapodial cirrus; pl, pydigial lobe; po, posterior field of sensory cilia; pr, prostomium; vb, ventral ciliary band; vt, ventral ciliary tufts; I–VIII, segments I–VIII

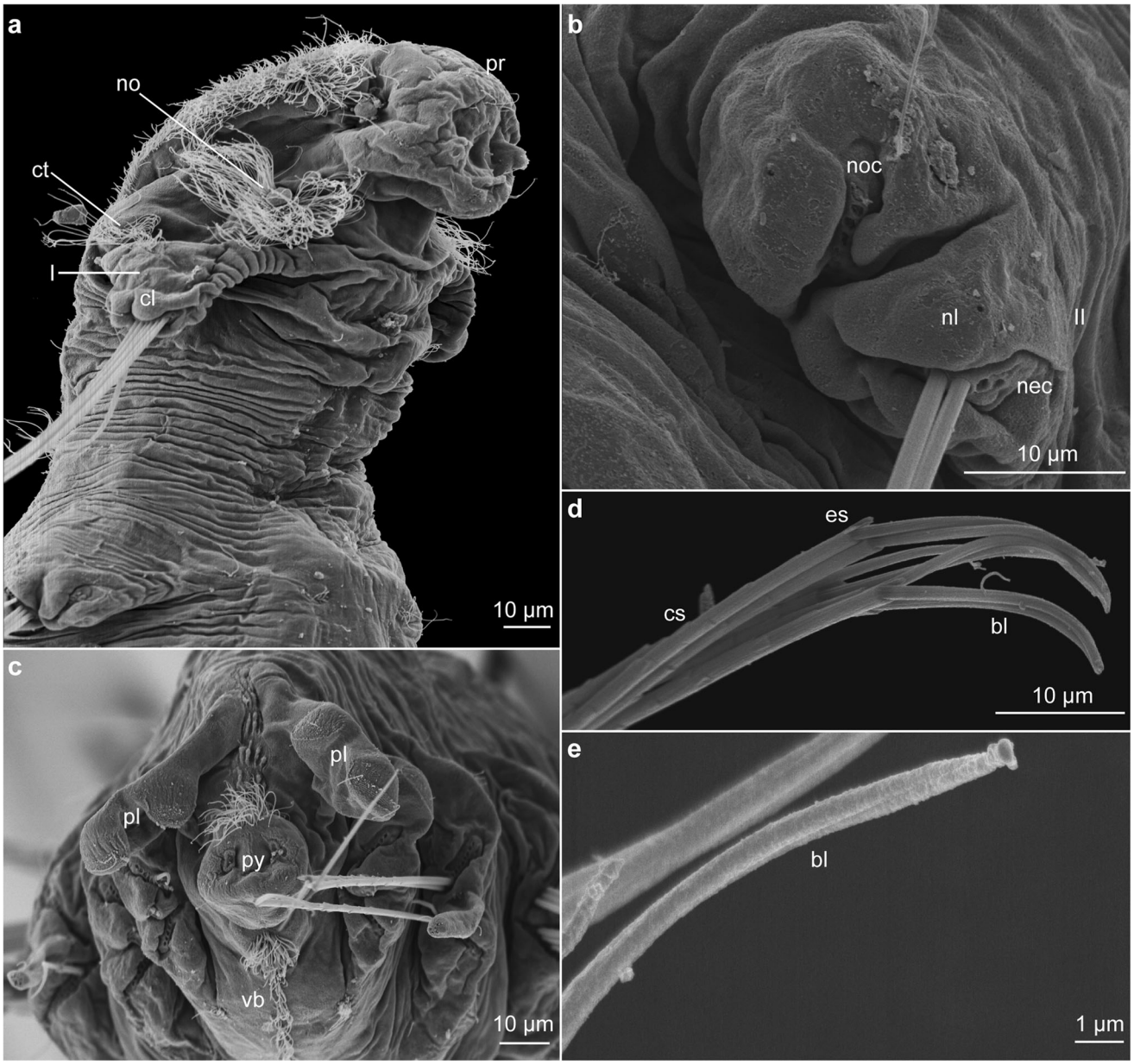

Fig. 6 *Speleonerilla salsa* sp. n. Scanning electron micrographs of **a** prostomium in ventrolateral view; **b** detail of segment II with neuropodial chaetal lobe in lateral view; **c** detail of pygidium with pygidial lobes and scars from pygidial cirrus, posterior view; **d** detail of chaetae with shaft, extension of shaft, and blade; **e** closer view of chaetal blade. bl, chaetal blade; cl, chaetal lobe; cs, chaetal shaft; ct, cilary tufts; es, extension shaft; nec, neurochaetae (chaetal holes, since chaetae are missing); nl, neuropodial chaetal lobe; no, nuchal organs; noc, notopodial chaetae (chaetal holes, since chaetae are missing); pl, pydigial lobe; pr, prostomium; py, pygidial cirrus; vb, ventral ciliary band; I–VIII, segments I–VIII

opening (versus two separate ventrolateral openings), and parapodial cirri present on all segments (see Table 3). Genetic distances to the other species of the genus are summarized in Table 4.

Phylogenetic analyses

Maximum likelihood and Bayesian analyses of our four concatenated markers (Table 1) yielded identical

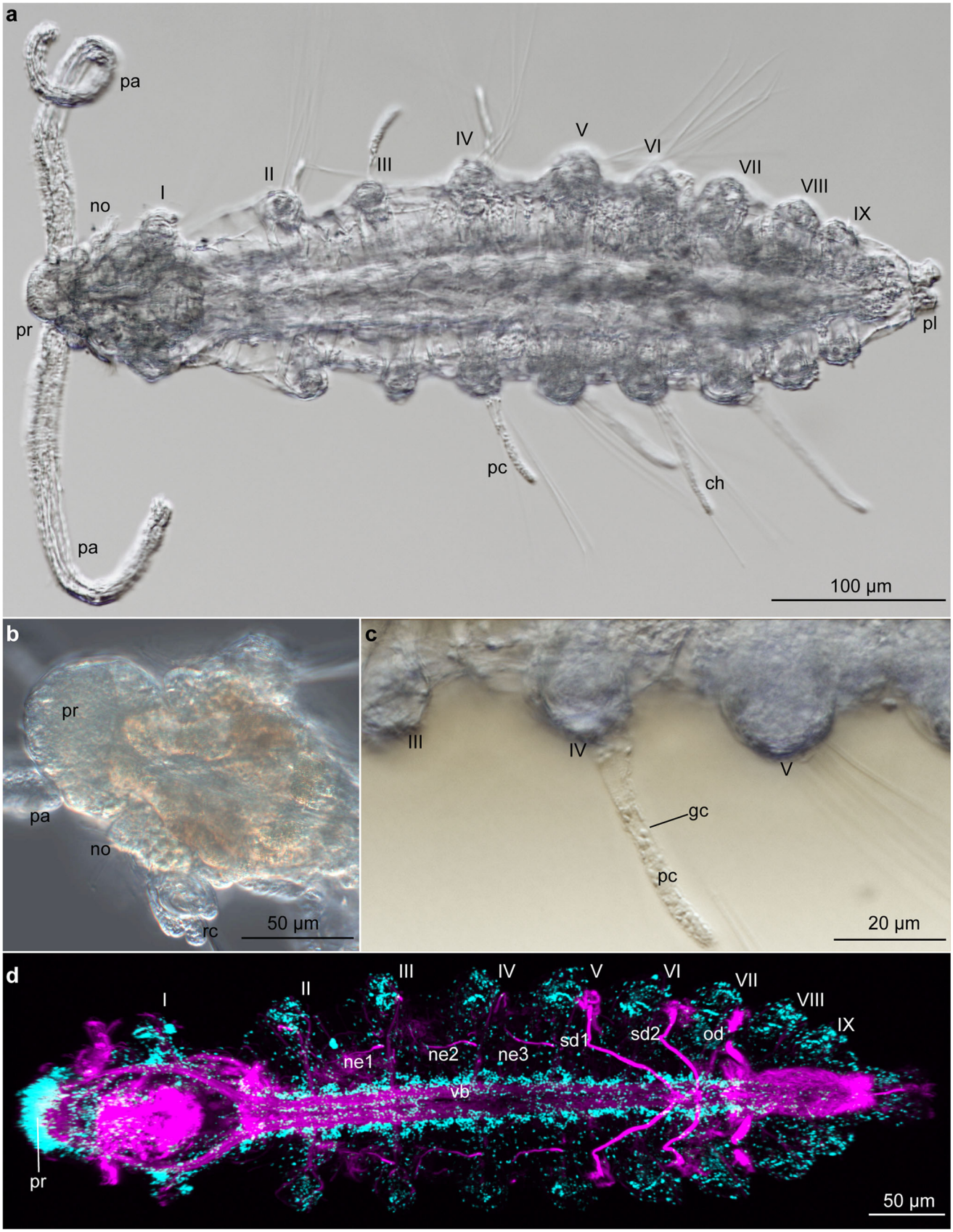
a
pa
I
II
III
IV
V
VI
VII
VIII
IX
no
pr
pl
pc
ch
pa
100 µm
b
pr
pa
no
rc
50 µm
c
III
IV
V
gc
pc
20 µm
d
I
II
III
IV
V
VI
VII
VIII
IX
ne1
ne2
ne3
sd1
sd2
od
vb
pr
50 µm

◀ **Fig. 7** *Speleonerilla isa* sp. n. Light microscopy images of **a** whole specimen with both palps in dorsal view; **b** prostomium and segment I with nuchal organs and rudimental cirri; **c** detail of interramal parapodial cirrus on segment IV; **d** maximum intensity projection of CLSM image stack showing segmentally arranged nephridia, oviducts, and spermioducts in ventrolateral view (pink—acetylated α-tubulin-like immunoreactivity, cyan—DAPI). ch, chaetae; gc, glandular cells; ne1–3, segmental nephridia; no, nuchal organs; od, oviduct; pa, palps; pc, parapodial cirrus; pl, pygidial lobe; pr, prostomium; rc, rudimental cirrus; sd1–2, spermioduct; vb, ventral ciliary band; I–XI, segments I–IX

topologies but with varying maximum likelihood bootstrap values (MLB) and Bayesian posterior probabilities (BPP) (Fig. 10). A monophyletic clade including all species of *Speleonerilla* was recovered in both analyses but not with full support (BPP/MLB: 0.84/99). The geographically distant *S. isa* was found to branch off next to a fully supported clade with the remaining species of *Speleonerilla*. The internal relationships of the Caribbean and Bermudian species are poorly supported, except for the fully supported nesting of the south Cuban species, *S. salsa* with *S. saltatrix* from Bermuda.

Discussion

Morphological features of *Speleonerilla*

All new species of *Speleonerilla* possess similar, extremely long flexible palps and ciliated lobular projections of the pygidium, such as described for *S. saltatrix*, hereof established to represent unique synapomorphies of all members of the genus. It seems unlikely that the pygidial lobes are modifications of the last segment or pygidial cirri (Worsaae et al. 2004), since they are also present in *S. isa* having nine segments and the easily shed pygidial cirri (or scars hereof) are now found in all new species in addition to the pygidial lobes. We also observed morphological and genetic differences, distinguishing them from *S. saltatrix*. *Speleonerilla isa* from La Corona lava tube in Lanzarote deviates the most, as it possesses nine segments and two pairs of spermioducts (with midventral openings) and it was consistently recovered as sister group of the remaining *Speleonerilla*. This phylogenetic position and multiple morphological differences could justify the placement of *S. isa* in a different genus. However, we preferred to keep it within *Speleonerilla* in order to avoid the description of a monotypic genus, which otherwise would present several of the same unique features (e.g., palps, lobes) characterizing *Speleonerilla*.

Secondary adaptations to suspension feeding

The presence of long ciliated palps, a body with transverse rows of ciliary tufts, and ciliated pygidial lobes facilitate swimming and suspension-feeding behavior in all species of the genus. In vitro observations of live *S. saltatrix* collected with plankton nets in the shallow, small entrance pool of Roadside Cave, Bermuda, revealed exceptional swimming skills compared to other nerillids (Worsaae et al. 2004, 2009) and indicated a semi- or fully swimming (holopelagic) lifestyle. Subsequent cave diving collecting of the here described additional species from larger water bodies with further distances to the bottom confirms that species of *Speleonerilla* are fully specialized to live up in the water column of anchialine caves, sometimes near the halocline. This grants access to the detritus and bacteria carried by tidal currents or caught within the haloclines of anchialine caves. The here presented collections in Northeast Cuba and the Yucatán Peninsula of México revealed *Speleonerilla* sp. A and *Speleonerilla* sp. B to be found both below and above the halocline in salinities down to 5 and 0‰, respectively (Worsaae, pers. obs). This indicates a further adaptive ability of *Speleonerilla* to cope with fast and drastically changing salinities (from 5 to 35‰ over short distances).

Colonization of the water column in anchialine systems

Species of *Speleonerilla* described herein have been collected from caves with very different morphology, geological age, history, and hydrology (Iliffe and Bishop 2009), although they are all being categorized as anchialine (Stock et al. 1986). The mid-Atlantic island of Bermuda sits atop an extinct Meso-Cenozoic seamount capped with Pleistocene limestone (Coates et al. 2013). The broad flat-topped platforms of the Bahamas archipelago, Cuba, and Yucatán Peninsula consist of thick layers of shallow water carbonates overlying crust associated with the opening of the North Atlantic basin in the Middle Jurassic (Williams et al. 1988; Bauer-Gottwein et al. 2011). Bermudian and Caribbean caves are near to the coast in Pleistocene age limestone. Coincidently, all four of these localities have well-developed brackish and saltwater layers separated by a halocline, where organic matter accumulates favoring the growth of chemoautotrophic bacteria that provides food into the system. In

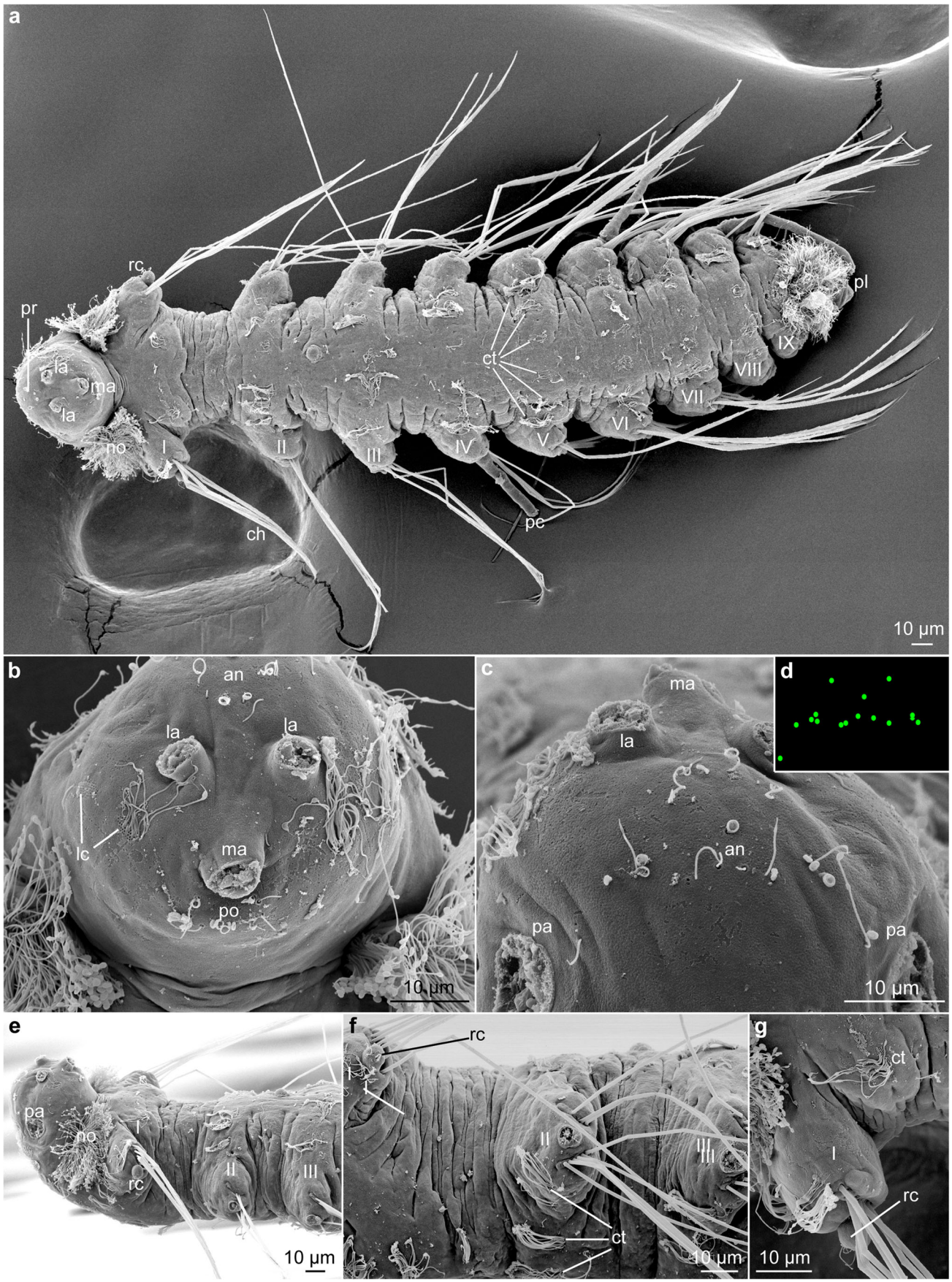
a
rc
pr
la
ma
la
no
I
II
III
IV
V
VI
VII
VIII
IX
ct
pl
ch
pc
10 μm
b
an
la
la
lc
ma
po
10 μm
c
ma
la
an
pa
pa
10 μm
d
e
pa
no
I
II
III
rc
10 μm
f
rc
I
II
III
ct
10 μm
g
ct
I
rc
10 μm

◀ **Fig. 8** *Speleonerilla isa* sp. n. Scanning electron micrographs of **a** whole specimen (both palps lost) in dorsal view; **b** prostomium with scars from lateral and median antennae, antero-dorsal view; **c** anterior view of prostomium showing anterior field of sensory cilia (as); **d** mapping of as; **e** prostomium and segments I–III in lateral view; **f** segments I–III in lateral view; **g** segment I with rudimental cirrus in ventral view. an, anterior field of sensory cilia; ch, chaetae; ct, ciliary tufts; la, lateral antenna; lc, prostomial lateral ciliation; ma, median antenna; no, nuchal organs; pa, palps; pc, parapodial cirri; pl, pydigial lobe; po, posterior field of sensory cilia; pr, prostomium; rc, rudimental cirri; I–XI, segments I–IX

contrast, the Lanzarote lava tube is of geologically recent and strictly volcanic in origin, with the cave lacking significant amounts of fresh or brackish water and exhibiting only a slight drop in salinity related to the tidal cycle (Wilkens et al. 2009). Despite of the lack of haloclines, the high porosity of the surrounding volcanic material and strong tidal currents favor the flow of suspended organic matter, preventing its deposition. In spite of the differences, the hydrology in all of these investigated cave systems supports a constant supply of suspended food sources, making the water column a more generous food niche than the nutrient-poor sediment layers (Pohlman et al. 1997; Iliffe et al. 2000; Martínez et al. 2016, 2017; Brankovits et al. 2017), which may be the driving force behind the radical evolutionary changes of the *Speleonerilla* morphology compared to other nerillids.

Other lineages of suspension-feeding animals have colonized the water column of the lava tube, including various groups of copepods, ostracods, amphipods, and thermosbaenaceans (Martínez et al. 2016). Among annelids, secondary adaptations toward swimming and suspension feeding are also found in the protodrilid *Megadrilus pelagicus* Martínez et al. 2017, endemic from Lanzarote and belonging to an otherwise interstitial genus (Martínez et al. 2015). Live observations of this species in aquaria and from inside the cave revealed them drifting in the water column upheld by the antiplectic metachronal beating of specialized ciliary bands (Martínez et al. 2017). Likewise, several macrofaunal cave annelids belonging to benthic marine lineages have also evolved swimming capabilities using muscular movements, e.g., the presumed suspension feeder *Speleobregma lanzaroteum* Bertelsen, 1986 of the family Scalibregmatidae (Martínez et al. 2012, 2013). The presence of all these suspension-feeding annelids possibly favors pelagicism of otherwise benthic, predatory species, such as the scale worms *Pelagomacellicephala* and *Gesiella* (Gonzalez et al. 2017, 2018a, b).

Diversification of the genus *Speleonerilla*

In the present study, members of *Speleonerilla* have been found at both sides of the Atlantic. The only species discovered in the East Atlantic, *S. isa*, was recovered as sister branch to the West Atlantic clade. This relationship is congruent with the morphological differences found between *S. isa* and the Caribbean clade. Many animal lineages exclusive from anchialine caves show similar disjunct distribution patterns to *Speleonerilla*, with representatives at both sides of the Atlantic and the Indo-Pacific (e.g., remipedes, thermosbaenaceans, leptanthurid isopods, atyids of the so-called TST clade, and thaumatociprid ostracods; Kornicker and Iliffe 1998; Koenemann et al. 2007; Koenemann et al. 2009; Page et al. 2018; Jurado-Rivera et al. 2017). The extremely disjunct distribution patterns of these taxa have been proposed to be a consequence of cave colonization during the Mesozoic, followed by vicariance (e.g., Stock 1981; Iliffe et al. 1984; Notenboom 1991; Humphreys 1993; Holsinger 1994; Koenemann and Holsinger 1999). However, the presence of several stygobites in geologically recent caves, such as Lanzarote, Christmas Island, or Bermuda (Sket and Iliffe 1980; Iliffe et al. 1983, 1984; Brankovits et al. 2017), and recent phylogenetic analyses (Botello et al. 2013; Jurado-Rivera et al. 2017) imply that dispersal may also have been involved. The deep sea has been classically suggested as a migratory pathway, as many of these cave-exclusive lineages exhibit deep-sea affinities (Hart et al. 1985; Gonzalez et al. 2017, 2018b), or alternatively larval dispersal throughout the open ocean may have been involved (Kano and Kase 2004; Jurado-Rivera et al. 2017). Without a molecular clock, our topology of *Speleonerilla* could be explained by any of these evolutionary scenarios, or a combination thereof.

The relationships among the West Atlantic species of *Speleonerilla* are poorly resolved, and the few resolved nodes do not reflect the geographical distances. Although this may be due to the lack of resolution of the markers, these markers seem appropriate to resolve the relationships among the remaining genera and species of Nerillidae (Worsaae and Martínez, unpublished). This suggest that either the lack of sampling in the Caribbean and Bermuda area and/or a rapid diversification process connected to the colonization of caves is reducing the resolution of our analyses, warranting further research throughout the Caribbean.

Fig. 9 *Speleonerilla isa* sp. n. Scanning electron micrographs of **a** ciliary tufts on segments VI–VII in dorsal view; **b** segments VIII–IX in dorsal view; **c** chaetae with shaft, extension of shaft, and blade. bl, chaetal blade; cs, chaetal shaft; ct, cilary tufts; es, extension shaft; pl, pydigial lobe; VI–XI, segments VI–IX

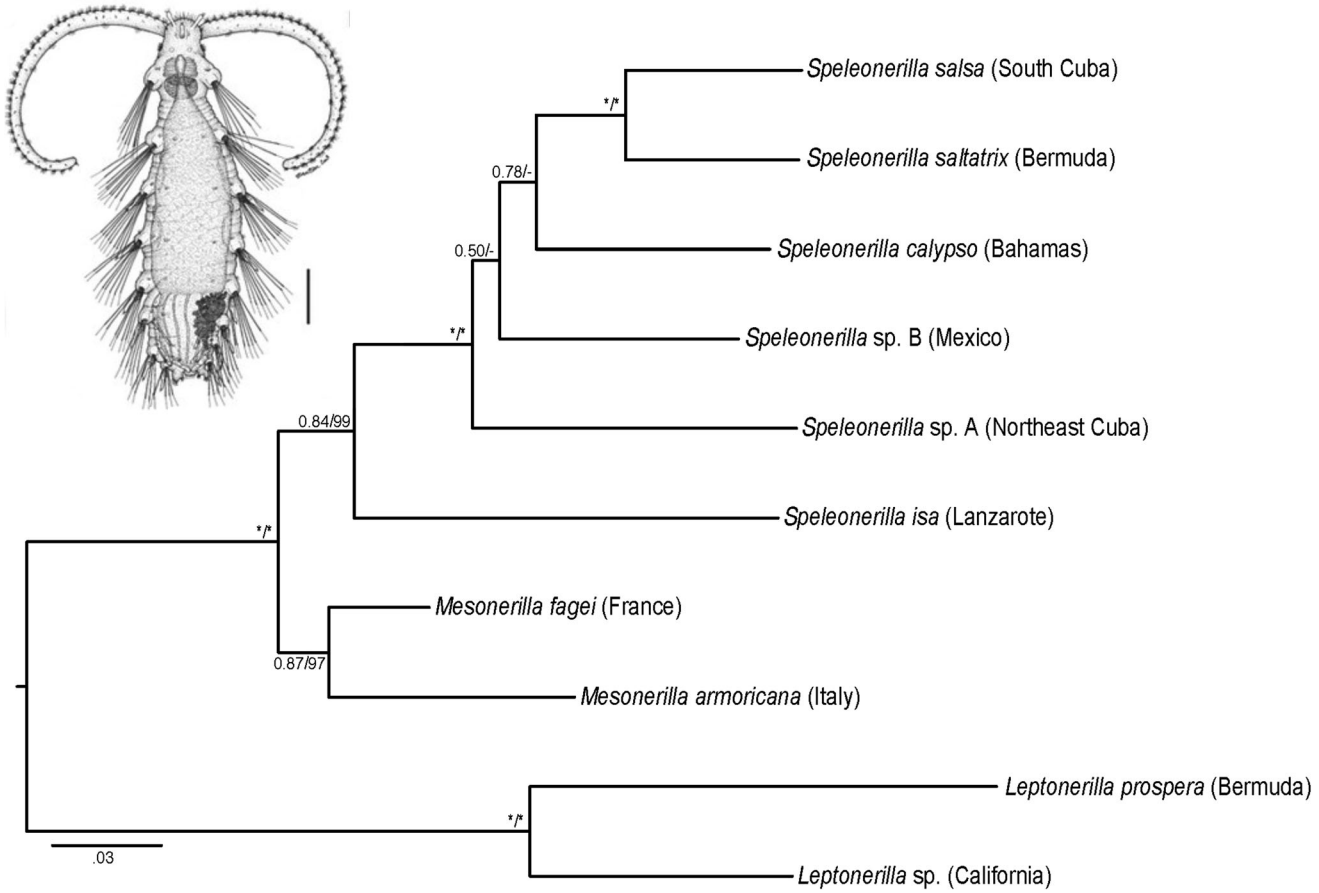

Fig. 10 Phylogenetic relationships of *Speleonerilla* spp. Tree topology based on concatenated gene dataset of four markers (COI, 18S, 28S, H3). Tree topologies were similar between maximum likelihood and Bayesian analyses. Only nodal support of Bayesian posterior probabilities (BPP) ≥ 0.5 and maximum likelihood bootstrap (MLB) ≥ 50 are presented. Nodes not recovered or with low support are represented by a dash (-). Asterisks (*) denote BPP = 1.0 and MLB = 100. Summary of the species and genes included in this phylogeny are listed in Table 1. Drawing of *Speleonerilla saltatrix* (Worsaae et al. 2004), scale bar 100 μm

Acknowledgements We are grateful to Elena Mateo and Leopoldo Moro for the assistance with obtaining the permissions. Special thanks go to the divers Luis E. Cañadas, Enrique Domínguez, Carola D. Jorge, Ralf Schoenemark, and a larger group of international students and colleagues helping us collect and sort out the animals during the First International Workshop to Marine and Anchialine Meiofauna, Lanzarote 2011.

Collection permits for the Bahamas were facilitated by Nancy Albury and Keith Tinker of The National Museum of the Bahamas/The Antiquities, Monuments and Museums Corporation (AMMC), and by the Abaco-based nongovernmental organization Friends of the Environment. A debt of gratitude goes out to Brian Kakuk (Bahamas Underground) as well as the additional cave divers assisting collections, including Lara Hinderstein, Tami Thomsen (Wisconsin Historical Society), and Gregg Stanton (Wakulla Diving Center). Jørgen Olesen (National History Museum Denmark, University of Copenhagen) sorted out and fixed precious samples for CLSM in the field, hereby allowing us to examine the nephridia of *S. calypso*, for which we are most grateful.

Provision of collection permits in México was facilitated by Fernando Álvarez, Universidad Nacional Autónoma de México to Thomas M. Iliffe (Texas A&M University at Galveston) and collecting was supported financially by grants of the Carlsberg Foundation as well as by the University of Copenhagen.

Collections during two expeditions in Cuba were supported by the Carlsberg Foundation and by an amazing group of divers, colleagues, and students from the Universities of Copenhagen and Havana: Peter Rask Møller, Arturo Regis, Erik García, José Andrés Pérez, Pedro Chevalier, Víctor Isla, Haidi Cecilie Petersen, and Maria Mikkelsen.

Funding Funding of the more than seven expeditions over 8 years was made possible through numerous agencies with the most recent laboratory and expedition costs to Cuba and México being covered by the Carlsberg Foundation (grants: 2013_01_0779 to AM and CF_0946 and 2013_01_0501 to KW) as well as supported through salaries and administration of the University of Copenhagen to KW, BCG, and colleagues.

Collections in Lanzarote and secondary laboratory costs were financially supported by the Danish Research Council (grant no. 272–06–0260 to KW) and the Carlsberg Foundation (2010_01_0802 to KW) as well as Consejería de Medio Ambiente del Gobierno de Lanzarote and authorized by Gobierno de Canarias and Centros Turísticos.

Collections in Bahamas received support from the National Science Foundation's Division of Environmental Biology (NSF DEB-9870219 and DEB-0315903), NOAA's Caribbean Marine Research Center, and the National Geographic Channel to TMI.

Compliance with ethical standards

Conflict of interest The authors declare that they have no conflict of interest.

Ethical approval All applicable international, national, and/or institutional guidelines for the care and use of animals were followed.

Sampling and field studies All necessary permits for sampling and observational field studies have been obtained by the authors from the competent authorities and are mentioned in the acknowledgements, if applicable.

References

Bauer-Gottwein P, Gondwe BR, Charvet G, Marín LE, Rebolledo-Vieyra M, Merediz-Alonso G (2001) The Yucatan Peninsula karst aquifer, Mexico. Hydrogeol J 19(3):507–524

Botello A, Iliffe TM, Álvarez F, Juan C, Pons J, Jaume D (2013) Historical biogeography and phylogeny of *Typhlatya* cave shrimps (Decapoda: Atyidae) based on mitochondrial and nuclear data. J Biogeogr 40(3):594–607

Brankovits D, Pohlman JW, Niemann H, Leigh MB, Leewis MC, Becker KW, Iliffe TM, Álvarez F, Lehmann MF, Phillips B (2017) Methane- and dissolved organic carbon-fueled microbial loop supports a tropical subterranean estuary ecosystem. Nat Commun 8: 1835

Brown S, Rouse G, Hutchings P, Colgan D (1999) Assessing the usefulness of histone H3, U2 snRNA and 28S rDNA in analyses of polychaete relationships. Aust J Zool 47:499–516

Coates KA, Fourqurean JW, Kenworthy WJ, Logan A, Manuel SA, Smith SR (2013) Introduction to Bermuda: geology, oceanography and climate. In: Sheppard C (ed) Coral reefs of the United Kingdom overseas territories. Coral reefs of the world, vol 4. Springer, Dordrecht

Cohen BL, Améziane N, Eleaume M, de Forges BR (2004) Crinoid phylogeny: a preliminary analysis (Echinodermata: Crinoidea). Mar Biol 144(3):605–617

Colgan DJ, McLauchlan A, Wilson GDF, Livingston SP, Edgecombe GD, Macaranas J, Cassis G, Gray MR (1998) Histone H3 and U2 snRNA DNA sequences and arthropod molecular evolution. Aust J Zool 46:419–437

Curini-Galletti M, Artois T, Delogu V, De Smet WH, Fontaneto D, Jondelius U, Leasi F, Martínez A, Meyer-Wachsmuth I, Nilsson KS, Tongiorgi P, Worsaae K, Todaro MA (2012) Patterns of Diversity in Soft-Bodied Meiofauna: Dispersal Ability and Body Size Matter. PLoS ONE 7(3):e33801

Felsenstein J (1985) Confidence limits on phylogenies: an approach using the bootstrap. Evolution 39(4):783–791

Folmer O, Black M, Hoeh W, Lutz R, Vrijenhoek R (1994) DNA primers for amplification of mitochondrial cytochrome c oxidase subunit I from diverse metazoan invertebrates. Mol Mar Biol Biotechnol 3(5): 294–299

Gerovasileiou V, Martínez A, Álvarez F, Boxshall G, Humphreys WF, Jaume D, Becking LE, Muricy G, van Hengstum PJ, Dekeyzer S, Vanhoorne B, Vandepitte L, Bailly N, Iliffe TM (2016) World Register of marine Cave Species (WoRCS): a new thematic species database for marine and anchialine cave biodiversity. RIO 2:e10451

Giribet G, Carranza S, Baguñá J, Riutort M, Ribera C (1996) First molecular evidence for the existence of a Tardigrada + Arthropoda clade. Mol Biol Evol 13(1):76–84

Gonzalez BC, Iliffe TM, Macalady JL, Schaperdoth I, Kakuk B (2011) Microbial hotspots in anchialine blue holes: initial discoveries from the Bahamas. Hydrobiol 677(1):149–156

Gonzalez BC, Martínez A, Borda E, Iliffe TM, Fontaneto D, Worsaae K (2017) Genetic spatial structure of an anchialine cave annelid indicates connectivity within—but not between—islands of the Great Bahama Bank. Mol Phylogenet Evol 109:259–270

Gonzalez BC, Worsaae K, Fontaneto D, Martínez A (2018a) Anophthalmia and elongation of body appendages in cave scale worms (Annelida: Aphroditiformia). Zool Scr 47:106–121. https://doi.org/10.1111/zsc.12258

Gonzalez BC, Martínez A, Borda E, Iliffe TM, Eibye-Jacobsen D, Worsaae K (2018b) Phylogeny and systematics of Aphroditiformia. Cladistics 34(3):225–259. https://doi.org/10.1111/cla.12202

Hall TA (1999) BioEdit: a user-friendly biological sequence alignment editor and analysis program for Windows 95/98/NT. Nucleic Acids Symp Ser 41:95–98

Hart CW, Manning RB, Iliffe TM (1985) The fauna of Atlantic marine caves: evidence of dispersal by sea floor spreading while maintaining ties to deep water. Proc Biol Soc Wash 98(1):288–292

Hillis DM, Dixon MT (1991) Ribosomal DNA: molecular evolution and phylogenetic inference. Q Rev Biol 66(4):411–453

Holsinger JR (1994) Pattern and process in the biogeography of subterranean amphipods. Hydrobiol 287(1):131–145

Humphreys WF (1993) Stygofauna in semi-arid tropical Western Australia: a Tethyan connection? Mem Biospeol 20:111–116

Ibrahim AK, Gamil IS, Abd-El baky AA, Hussein MM, Tohamy AA (2011) Comparative molecular and conventional detection methods of *Babesia equi* (*B. equi*) in Egyptian equine. Glob Vet 7(2):201–210

Iliffe TM, Bishop RE (2009) Adaptations to life in marine caves. In: Safran P (ed) Fisheries and aquaculture, encyclopedia of life support systems, vol 5. Eolss Publishers, Oxford, pp 183–205

Iliffe TM, Kornicker L (2009) Worldwide diving discoveries of living fossil animals from the depths of anchialine and marine caves. Smithson Contrib Mar Sci 38:269–280

Iliffe TM, Hart CW Jr, Manning RB (1983) Biogeography and the caves of Bermuda. Nature 302:141–142

Iliffe TM, Wilkens H, Parzefall J, Williams D (1984) Marine lava cave fauna: composition, biogeography and origins. Science 225(4659): 309–311

Iliffe TM, Parzefall J, Wilkens H (2000) Ecology and species distribution of the Monte Corona lava tunnel on Lanzarote (Canary Islands). In: Wilkens H, Culver DC, Humphreys WF (eds) Subterraean ecosystems, ecosystems of the world. 30:633–644

Jouin C (1973) Nouvelles données sur *Troglochaetus beranecki* Delachaux (Archiannelida Nerillidae). Ann Spéléol 28:575–579

Jurado-Rivera JA, Pons J, Alvarez F, Botello A, Humphreys WF, Page TJ, Iliffe TM, Willansen E, Meland K, Jaume D (2017) Phylogenetic

evidence that both ancient vicariance and dispersal have contributed to the biogeographic patterns of anchialine cave shrimps. Sci Rep 7: 2852

Kano Y, Kase T (2004) Genetic exchange between anchialine cave populations by means of larval dispersal: the case of a new gastropod species *Neritilia cavernicola*. Zool Scr 33(5):423–437

Katoh K, Toh H (2008) Recent developments in the MAFFT multiple sequence alignment program. Brief Bioinform 9(4):286–298

Katoh K, Kuma KI, Toh H, Miyata T (2005) MAFFT version 5: improvement in accuracy of multiple sequence alignment. Nucleic Acids Res 33(2):511–518

Katoh K, Asimenos G, Toh H (2010) Multiple alignment of DNA sequences with MAFFT. In: Posada D (ed) Bioinformatics for DNA sequence analysis. Methods in molecular biology (methods and protocols) 537. Humana, New York, pp 39–64

Koenemann S, Holsinger JR (1999) Phylogenetic analysis of the amphipod crustacean family Bogidiellidae, s. lat., and revision of taxa above the species level. Crustaceana 72(8):781–816

Koenemann S, Schram FR, Hönemann M, Iliffe TM (2007) Phylogenetic analysis of Remipedia (Crustacea). Org Divers Evol 7(1):33–51

Koenemann S, Bloechl A, Martínez A, Iliffe TM, Hoenemann M, Oromí P (2009) A new, disjunct species of *Speleonectes* (Remipedia, Crustacea) from the Canary Islands. Mar Biodivers 39:215–225

Kornicker LS, Iliffe TM (1998) Myodocopid Ostracoda (Halocypridina, Cladocopina) from anchialine caves in the Bahamas, Canary Islands, and Mexico. Smithson Contrib Zool 599:1–93

Levinsen GMR (1883) Systematisk-geografisk Oversigt over de nordiske Annulata, Gephyrea, Chaetognathi og Balanoglossi. Vid Medd Dansk Naturhist For, København 1882:160–251

Lovejoy C, Potvin M (2011) Microbial eukaryotic distribution in a dynamic Beaufort Sea and the Arctic Ocean. J Plankton Res 33(3): 431–444

Markmann M (2000) Entwicklung und Anwendung einer 28S rDNA-Sequenzdatenbank zur Aufschlüsselung der Artenvielfalt limnischer Meiobenthosfauna im Hinblick auf den Einsatz moderner Chiptechnologie. PhD thesis, University of Munich, Germany

Martínez A, Palmero AM, Brito MC, Núñez J, Worsaae K (2009) Anchialine fauna of the Corona lava tube (Lanzarote, Canary Islands): diversity, endemism and distribution. Mar Biodivers 39(3):169–187

Martínez A, Di Domenico M, Worsaae K (2012) Gain of palps within a lineage of ancestrally burrowing annelids (Scalibregmatidae). Acta Zool (Stockholm) 95(4):421–429

Martínez A, Di Domenico M, Worsaae K (2013) Evolution of cave *Axiokebuita* and *Speleobregma* (Scalibregmatidae, Annelida). Zool Scr 42(6):623–636

Martínez A, Di Domenico M, Rouse GW, Worsaae K (2015) Phylogeny of Protodrilidae (Annelida) inferred by total evidence analyses. Cladistics 31:250–276

Martínez A, Gonzalez BC, Núñez J, Wilkens H, Oromí P, Iliffe TM, Worsaae K (2016) Guide to the anchialine ecosystems of Los Jameos del Agua and Túnel de la Atlántida. Medio Ambiente, Cabildo de Lanzarote, Arrecife, Lanzarote, Spain, 310 pp., ISBN-13: 978-84-95938-92-3

Martínez A, Kvindebjerg K, Iliffe TM, Worsaae K (2017) Evolution of cave suspension feeding in Protodrilidae (Annelida). Zool Scr 46(2): 214–226

Meyer CP (2003) Molecular systematics of cowries (Gastropoda: Cypraeidae) and diversification patterns in the tropics. Biol J Linn Soc 79(3):401–459

Miller MA, Pfeiffer W, Schwartz T (2010) Creating the CIPRES Science Gateway for inference of large phylogenetic trees. Gateway Computing Environments Workshop (GCE)

Morselli I, Sarto M, Mari M (1998) *Troglochaetus beranecki* Delachaux (Annelida, Polychaeta): collecting methods and microscopy techniques for SEM and in vivo observations. Hydrobiol 379(1–3):213–216

Notenboom J (1991) Marine regressions and the evolution of groundwater dwelling amphipods (Crustacea). J Biogeogr 18(4):437–454

Núñez J, Ocaña O, Brito MC (1997) Two new species (Polychaeta: Fauveliopsidae and Nerillidae) and other polychaetes from the marine lagoon cave of Jameos del Agua, Lanzarote (Canary Islands). Bull Mar Sci 60(2):252–260

Page TJ, Hughes JM, Real KM, Stevens MI, King RA, Humphreys WF (2018) Allegory of a cave crustacean: systematic and biogeographic reality of *Halosbaena* (Peracarida: Thermosbaenacea) sought with molecular data at multiple scales. Mar Biodivers 48(2):1185–1202

Pennak RW (1971) A fresh-water archiannelid from the Colorado Rocky Moutains. Trans Am Microsc Soc 90(3):372–375

Plesa C (1977) Nouvelles données sur la répartition et l'écologie de *Troglochaetus beranecki* Delachaux (Archiannelida) en Roumanie. Trav Inst Spéol 16:9–16

Pohlman JW, Iliffe TM, Cifuentes LM (1997) A stable isotope study of organic cycling and the ecology of an anchialine cave ecosystem. Mar Ecol Prog Ser 155:17–27

Posada D (2008) jModelTest: phylogenetic model averaging. Mol Biol Evol 25(7):1253–1256

Posada D, Buckley TR (2004) Model selection and model averaging in phylogenetics: advantages of Akaike information criterion and Bayesian approaches over likelihood ratio tests. Syst Biol 53(5): 793–808

Rambaut A, Drummond AJ (2007). Tracer v1. 4: MCMC trace analyses tool. In http://tree.bio.ed.ac.uk/software/tracer. Accessed 19 Dec 2016

Ronquist F, Huelsenbeck JP (2003) MrBayes 3: Bayesian phylogenetic inference under mixed models. Bioinformatics 19(12):1572–1574

Sambugar B (2004) La presenza di *Troglochaetus beranecki* Delachaux (Polychaeta, Nerillidae) in due grotte italiane. Studi Trent Sci Nat Acta Biol 81:145–148

Särkkä J, Mäkela J (1998) *Troglochaetus beranecki* Delachaux (Polychaeta, Archiannelida) in esker groundwaters of Finland: a new class of limnic animals for north Europe. Hydrobiol 379(1–3):17–21

Schneider CA, Rasband WS, Eliceiri KW (2012) NIH Image to ImageJ: 25 years of image analysis. Nature Met 9:671–675

Sket B, Iliffe TM (1980) Cave fauna of Bermuda. Int Rev Hydrobiol 65(6):871–882

Stamatakis A (2006) RAxML-VI-HPC: maximum likelihood-based phylogenetic analyses with thousands of taxa and mixed models. Bioinformatics 22(21):2688–2690

Sterrer W, Iliffe TM (1982) *Mesonerilla prospera*, a new archiannelid from marine caves in Bermuda. Proc Biol Soc Wash 95(3):509–514

Stock JH (1981) The taxonomy and zoogeography of the family of Bogidiellidae (Crustacea, Amphipoda), with emphasis on the West Indian taxa (Amsterdam expeditions to the West Indian Islands, report 14). Bijdr Dierk Amsterdam 51(2):345–374

Stock JH, Iliffe TM, Williams WD (1986) The concept of "anchialine" reconsidered. Stygologia 2(1/2):90–92

Tilzer M (1970) Hydrobiology of marginal caves. Part III. *Nerilla marginalis* n.sp. (Polychaeta Archiannelida) a recent immigrant into a marginal cave in Istra (Yugoslavia). Int Revue Ges Hydrobiol 55(2):221–226

Vaidya G, Lohman DJ, Meier R (2011) SequenceMatrix: concatenation software for the fast assembly of multi-gene datasets with character set and codon information. Cladistics 27(2):171–180

Walker F (1865) List Spec. lepid. Insects Colln Br Mus (31):195

Wilkens H, Iliffe TM, Oromí P, Martínez A, Tysall TN, Koenemann S (2009) The Corona lava tube, Lanzarote: geology, habitat diversity and biogeography. Mar Biodivers 39(3):155–167

Williams CF, Anderson RN, Austin JA Jr (1988) Structure and evolution of Bahamian deep-water channels: insights from *in-situ* geophysical

and geochemical measurements. In: Austin JA Jr, Schlager W et al (eds) Proc Ocean Drill Program Sci Res, vol 101, pp 439–451

Worsaae K (2005a) Systematics of Nerillidae (Polychaeta, Annelida). Meiofauna Mar 14:49–74

Worsaae K (2005b) Phylogeny of Nerillidae (Polychaeta, Annelida) as inferred from combined 18S rDNA and morphological data. Cladistics 21(2):143–162

Worsaae K (2014) Nerillidae Levinsen, 1883. In: Beutel RG, Kristensen NP, Leschen R, Purschke W, Westheide W, Zachos F (eds) Handbook of zoology online. Walter de Gruyter, Berlin

Worsaae K, Kristensen RM (2005) A new species of *Paranerilla* (Polychaeta: Nerillidae) from northeast Greenland waters, Arctic Ocean. Cah Biol Mar 44(1):23–39

Worsaae K, Müller MCM (2004) Nephridial and gonoduct distribution patterns in Nerillidae (Annelida: Polychaeta) examined by tubulin staining and cLSM. J Morph 261(3):259–269

Worsaae K, Rouse GW (2009) *Mesonerilla neridae* sp. nov. (Nerillidae): first meiofaunal annelid from deep-sea hydrothermal vents. Zoosymposia 2:297–303

Worsaae K, Sterrer W, Iliffe TM (2004) *Longipalpa saltatrix*, a new genus and species of the meiofaunal family Nerillidae (Annelida: Polychaeta) from an anchialine cave in Bermuda. Proc Biol Soc Wash 117(3):346–362

Worsaae K, Martínez A, Núñez J (2009) Nerillidae (Annelida) from the Corona lava tube, Lanzarote with description of *Meganerilla cesari* n. sp. Mar Biodivers 39(3):195–207